Xigaze forearc basin revisited (South Tibet): Provenance changes and origin of the Xigaze Ophiolite

Wei An[1], Xiumian Hu[1,†], Eduardo Garzanti[2], Marcelle K. BouDagher-Fadel[3], Jiangang Wang[4], and Gaoyuan Sun[1]
[1]*State Key Laboratory of Mineral Deposits Research, School of Earth Sciences and Engineering, Nanjing University, Nanjing, 210029, China*
[2]*Department of Earth and Environmental Sciences, Università di Milano-Bicocca, Milano, 20126, Italy*
[3]*Department of Earth Sciences, University College London, London, WC1E 6BT, UK*
[4]*Institute of Geology and Geophysics, Chinese Academy of Sciences, Beijing, 100029, China*

ABSTRACT

Our new stratigraphic, sedimentological, and micropaleontological analysis, integrated with basalt geochemistry, sandstone petrography, and detrital-zircon U-Pb and Hf isotope data, suggests the revision of current models for the geological evolution of the Asian active margin during the Cretaceous. The Xigaze forearc basin began to form in the late Early Cretaceous, south of the Gangdese arc, during the initial subduction of the Neotethyan oceanic lithosphere under the Lhasa terrane. Well-preserved stratigraphic successions document the classical upward-shallowing pattern of the forearc-basin strata and elucidate the origin of the associated oceanic magmatic rocks. The normal mid-ocean-ridge basalt (N-MORB) geochemical signature and stratigraphic contact with the overlying abyssal cherts (Chongdui Formation) indicate that the Xigaze Ophiolite formed by forearc spreading and represents the basement of the forearc sedimentary sequence. Volcaniclastic sedimentation began with thick turbiditic sandstones and interbedded shales in the late Albian–Santonian (Ngamring Formation) followed by shelfal, deltaic, and fluvial strata (Padana Formation), with final filling of the basin by the Campanian age. Forearc sandstones do not show the classical trend from feldspatholithic volcaniclastic to quartzo-feldspathic plutoniclastic compositions, indicating limited unroofing of the Gangdese arc prior to collision. U-Pb age spectra of detrital zircons are unimodal with a 107 Ma peak in the lower Ngamring Formation (104–99 Ma), bimodal with a subordinate additional peak at 157 Ma in the middle Ngamring Formation (99–88 Ma), and multimodal with more abundant pre-Mesozoic ages in the upper Ngamring and Padana Formations (88–76 Ma). These three petrofacies with distinct provenances document the progressive erosional evolution of the Gangdese arc, with uplift of the central Lhasa terrane and expanding river catchments to include the central Lhasa terrane during the Late Cretaceous.

INTRODUCTION

After the onset of oceanic subduction, an arc-trench system develops on the upper plate, evolves through time, and is finally terminated by the subsequent collisional or accretionary orogens (Dickinson, 1995; Cawood et al., 2011). The forearc-basin succession generally undergoes limited deformation, thereby preserving significant information regarding the origin of the forearc basement and the volcanic and erosional history of the magmatic arc. Forearc-basin studies are thus greatly helpful for understanding and reconstructing the evolution of the entire subduction system, as documented by the successful cases of the Great Valley basin in California (Ingersoll, 1978, 1979, 1982, 1983, 2012; DeGraaff-Surpless et al., 2002) and the forearc basin of the Terra Australis orogen in Australia (Cawood, 1983, 2005).

A belt of forearc basins formed along the southern margin of Asia during northward subduction of the Neotethys Ocean. Forearc-basin successions displaying the classic shallowing-upward trend from turbidites to shelfal and fluvio-deltaic sediments during the late Early Cretaceous to Late Cretaceous are well developed all along the Himalayas. From the Indus forearc basin in Ladakh (Garzanti and Van Haver, 1988) to the Xigaze forearc basin in South Tibet (Yin et al., 1988; Einsele et al., 1994; Dürr, 1996), superb rock exposures provide a splendid opportunity to reconstruct the subduction history of the Asian active margin (Fig. 1).

The biostratigraphy and sedimentology of the Xigaze forearc-basin succession were first established decades ago (Wen, 1974; Cao, 1991; Wu, 1984; Liu et al., 1988), and revised later on (Wan et al., 1997, 1998; Li et al., 2008a, 2008b). Lithofacies and provenance studies have been published by Dürr (1993, 1996) and Einsele et al. (1994), leading to the conclusion that detritus was dominantly derived from the Gangdese arc and Lower Cretaceous limestone of the Sangzugang Formation, with additional contributions from the Lhasa terrane in the north, as supported by detrital-zircon U-Pb ages and Hf isotopic data (Wu et al., 2010).

Several questions about the stratigraphy and sedimentology of the Xigaze forearc basin remain unanswered. Different opinions exist regarding the timing of initial forearc-basin development and the character of the oldest forearc-basin strata. Previous studies focused mostly on deep-sea turbidites and largely neglected the final stage of basin filling, characterized by shallow-marine and fluvio-deltaic sediments. The forearc basement has been studied insufficiently, and its origin remains to be ascertained. Einsele et al. (1994) interpreted the Xigaze Ophiolite as oceanic or transitional crust trapped during subduction, whereas Hébert et al. (2012) concluded that it formed above the subduction zone.

Our study includes: (1) the stratigraphic and sedimentological analysis of the entire Xigaze forearc-basin sequence; (2) the geochemical analysis of basaltic lavas underlying the sedimentary succession; and (3) provenance analysis by sandstone petrography integrated with detrital-zircon U-Pb and Hf isotopic data. Based on our new data, the evolution of the Xigaze forearc basin is reconsidered, and insights are

†E-mail: huxm@nju.edu.cn.

GSA Bulletin; November/December 2014; v. 126; no. 11/12; p. 1595–1613; doi: 10.1130/B31020.1; 14 figures; 2 tables; Data Repository item 2014236; published online 30 June 2014.

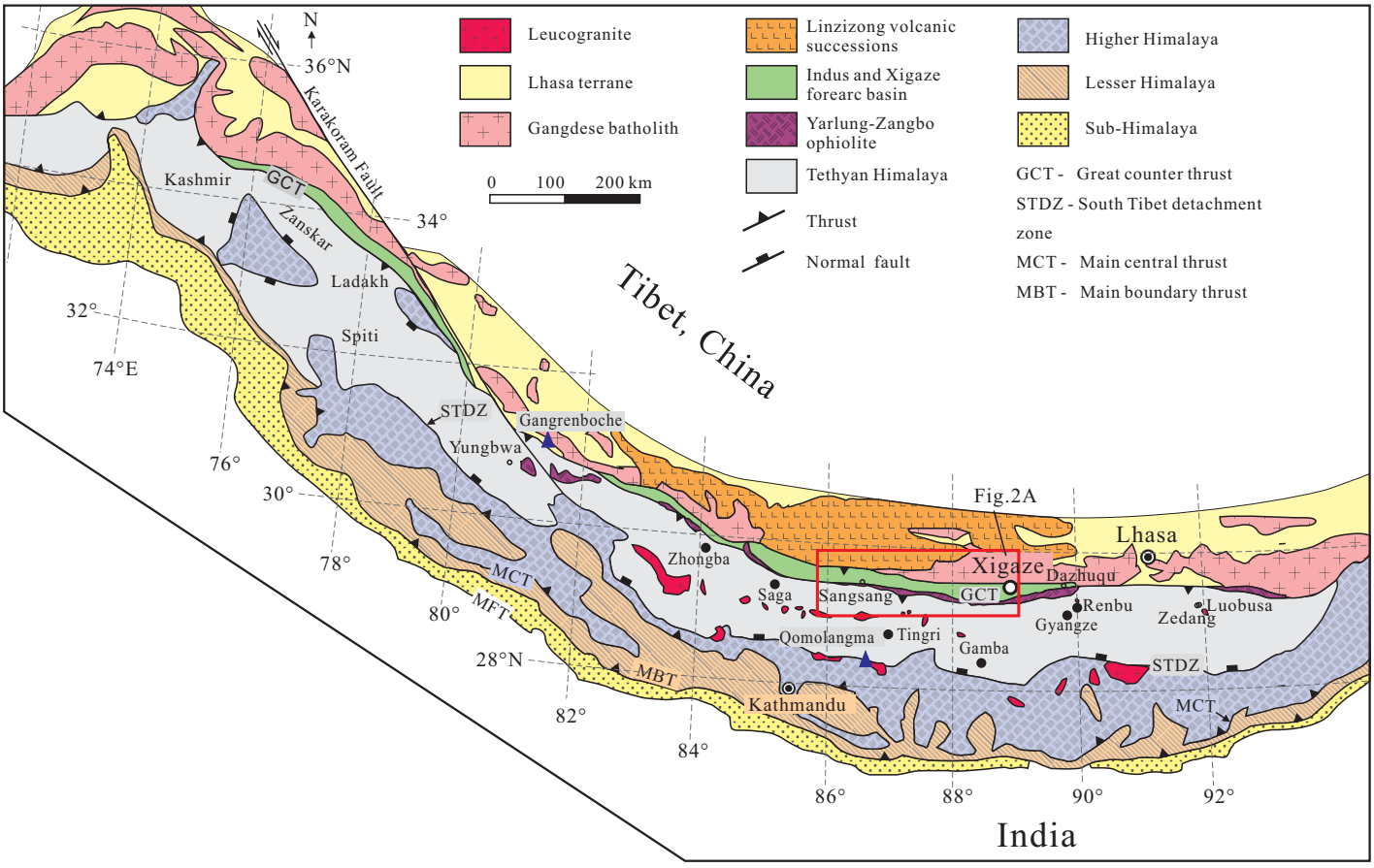

Figure 1. Simplified geologic map of the Himalaya (after Pan et al., 2004).

provided into the origin of the Xigaze Ophiolite and into the erosional evolution of the Gangdese arc and Lhasa terrane. Throughout the article, correlation between relative and absolute ages is based on the time scale of Gradstein et al. (2012).

GEOLOGICAL FRAMEWORK OF SOUTH TIBET

Tectonic Units

The Lhasa terrane is a W-E–trending tectonic belt that can be divided into northern, central, and southern subterranes characterized by different sedimentary rocks (Zhu et al., 2011). In the southern Lhasa terrane, the sedimentary cover is limited and mainly of Late Triassic–Cretaceous age (Pan et al., 2006; Zhu et al., 2008, 2013). Permian–Carboniferous metasedimentary and Upper Jurassic–Lower Cretaceous volcano-sedimentary strata are widespread in the central Lhasa terrane (Pan et al., 2004; Zhu et al., 2011, and references therein). In the northern Lhasa terrane, sedimentary rocks are mainly Jurassic and Cretaceous in age, with minor Triassic strata. Magmatic rocks emplaced in the southern and central Lhasa terranes from the Late Triassic to the Eocene (220–40 Ma) are characterized by distinct zircon U-Pb age spectra and Hf isotopes. The southern Lhasa terrane yields predominantly zircons with positive $\varepsilon_{Hf(t)}$ (Chu et al., 2006; Zhang et al., 2007a; Ji et al., 2009), whereas zircons with negative $\varepsilon_{Hf(t)}$ predominate in the central Lhasa terrane (Chu et al., 2006; Zhang et al., 2007b; Zhou et al., 2008; Zhu et al., 2011).

The Yarlung-Zangbo suture zone includes four tectonic units (from north to south; Ding et al., 2005): the Gangdese magmatic arc, the Xigaze forearc basin, the Yarlung-Zangbo Ophiolite, and the subduction complex (mélange) (Fig. 2A).

The Gangdese magmatic arc is a plutonic belt extending ~2500 km along the northern side of the Yarlung-Zangbo suture zone (Wen et al., 2008; Ji et al., 2009). Outcrops chiefly consist of granitoids emplaced between 103 and 42 Ma (Late Cretaceous–Eocene). Small bodies with Early Cretaceous to Jurassic ages as old as 190 Ma occur locally (Chu et al., 2006; Zhang et al., 2007a, 2007b). Jurassic–Lower Cretaceous volcano-sedimentary strata are also widespread (Yeba Formation and Sangri Group; Dong et al., 2006; Geng et al., 2006; Zhu et al., 2008).

The Yarlung-Zangbo Ophiolite crops out from Luobusa in the east to Yungbwa in the west; the central part between Dazhuqu and Sangsang is termed the Xigaze Ophiolite. The Yarlung-Zangbo Ophiolite is composed of mantle peridotites, cumulates, gabbros, sheeted dikes, pillow lavas, and radiolarian cherts. The age of magmatic rocks, previously assessed at 120 ± 10 Ma (Göpel et al., 1984), has since been refined to 123–128 Ma (Malpas et al., 2003; Xia et al., 2003; Dai et al., 2011a, 2011b, 2013). Formerly interpreted as having been produced by a slow-spreading mid-ocean ridge (Nicolas et al., 1981; Xiao, 1984; Girardeau et al., 1985a, 1985b), recent studies have favored formation in a suprasubduction setting (Bédard et al., 2009, 2011; Dai et al., 2011a; Hébert et al., 2012).

The subduction complex, in tectonic contact with the Yarlung-Zangbo Ophiolite along the Renbu-Zedang thrust fault and with Tethyan Himalayan strata in the south along the

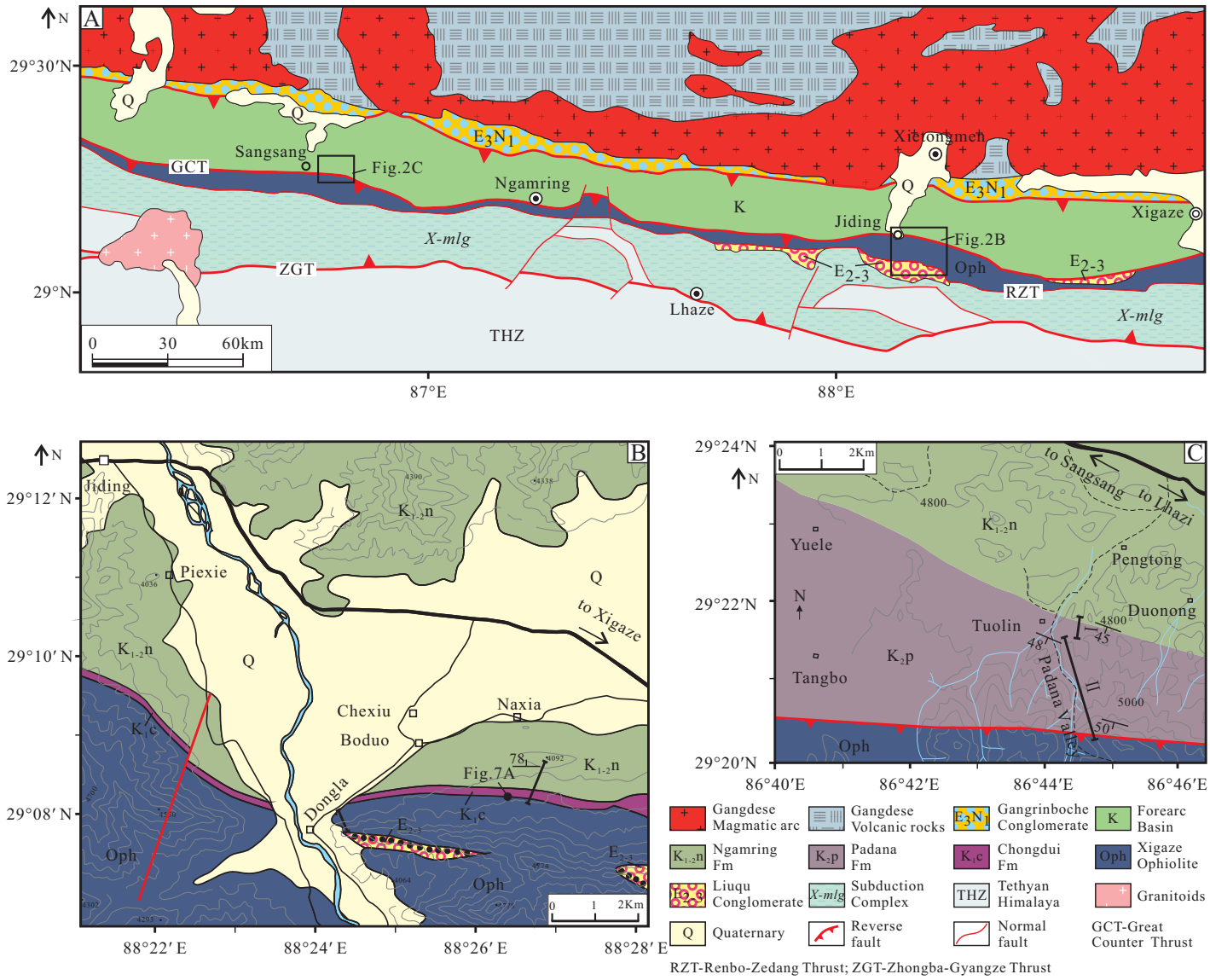

Figure 2. (A) Geological sketch map of the studied region and surrounding units (after Pan et al., 2004); (B) location of the Naxia section; (C) locations of the Padana sections. GCT—Great Counter Thrust.

Zhongba-Gyangze fault, has an exposed length of ~1000 km and width of 10–50 km. It consists of serpentinite-matrix mélange, mud-matrix mélange, and minor turbidites in the south (Pan et al., 2004; Cai et al., 2012). Outcrops of serpentinite-matrix mélange vary in width from several hundred meters to several kilometers and include up to kilometer-scale blocks of quartzite, chert, amphibolite, and mafic and ultramafic rocks. Mud-matrix mélange includes mudstone, chert, limestone, sandstone, and chert blocks.

Two distinct conglomerate belts are preserved along the Yarlung-Zangbo Ophiolite. The uppermost Oligocene–Lower Miocene Gangrinboche Conglomerate (23–18 Ma) is exposed south of the Gangdese magmatic arc and records a change of source areas from the Gangdese arc to both the Gangdese arc and the Himalayan orogen (Wang et al., 2013). The postcollisional Liuqu Conglomerate, exposed just south of the Yarlung-Zangbo Ophiolite, contains detritus derived from both the Indian and Asian continents (Wang et al., 2010).

Stratigraphy of the Xigaze Forearc Basin

The Xigaze forearc-basin succession, exposed from Renbu in the east to Zhongba in the west over a length of ~500 km and with a maximum width of ~22 km, is traditionally subdivided into five units, including the Chongdui, Sangzugang, Ngamring, and Padana Formations (XBGMR, 1997; Wang et al., 2012; GSA Data Repository, Table DR5[1]). The overlying Cuojiangding Group, representing the youngest deposit within the basin (Ding et al., 2005), is not exposed in the study area and is not considered here.

The Chongdui Formation, named after Chongdui, a village 20 km SE of Xigaze, was

[1]GSA Data Repository item 2014236, detrital modal composition, detrital-zircon U-Pb and Hf isotopic data, major- and trace-elements data, stratigraphic subdivisions, main lithofacies, sample locality information, location of the Sangzugang section, column of the Sangzugang Formation, and foraminifera associations, is available at http://www.geosociety.org/pubs/ft2014.htm or by request to editing@geosociety.org.

first described by Cao (1991) as including deep-water turbidites with detritus derived from magmatic-arc rocks and ophiolites. Subsequently, the unit was subdivided into two members: (1) purplish-greenish radiolarian chert interbedded with siliceous mudstone (73–97 m thick), overlain by (2) dark-gray thin-bedded sandstones and mudrocks, with minor limestones at the top (200 m thick; Wu, 1984; Ziabrev et al., 2003). The lower chert member contains a late Barremian–late Aptian radiolarian association (Ziabrev et al., 2003), whereas the overlying sandstone member contains detrital zircons with the youngest peak age of 116 Ma (late Aptian; Wu et al., 2010).

The Sangzugang Formation, named by Wu et al. (1977) after Sangzugang village (Sagya County, east of Xigaze) and exposed discontinuously from Sangzugang to the Xigaze airport, consists of thick-bedded or massive dark-gray bioclastic limestones with abundant benthic foraminifera, rudists, corals, and minor bivalves. The 60–230-m-thick Sangzugang Formation is in fault contact with either the Ngamring Formation or the Gangrinboche Conglomerate (Wang et al., 2013), and its original stratigraphic relationships are uncertain. The Sangzugang Formation was deposited in reefal environments along the northern part of the forearc basin during the late Aptian to early Albian (Liu et al., 1988). It can be considered an equivalent to the rudistid-bearing Khalsi Limestone of the Ladakh Himalaya, which is paraconformably overlain by volcaniclastic turbidites that contain ammonoids of the late Albian age at the base (Garzanti and Van Haver, 1988).

The Ngamring Formation, first defined in Ngamring County by Wu et al. (1977), represents the main turbiditic fill of the Xigaze forearc basin, with thicknesses between 1000 and 4000 m. Based on stratigraphic and structural analysis, Wang and Liu (1999) and Wang et al. (2012) identified five megasequences, including channelized conglomerates, turbiditic sandstones, and mudrocks with minor limestones and marls deposited in submarine-fan to slope environments. The Ngamring Formation forms an E-W–trending asymmetric synclinorium (Wan et al., 1998). It is in conformable stratigraphic contact with both the underlying Chongdui Formation and the overlying Padana Formation in the south, and locally in fault contact with the Xigaze Ophiolite in the south or the Gangrinboche Conglomerate in the north (Wang et al., 2012). Foraminiferal associations indicate Aptian–Albian and Cenomanian–Turonian ages for the oldest strata in the northern and southern flanks of the synclinorium, respectively, whereas the youngest ages along its axis are late Coniacian (Wan et al., 1998). This is consistent with the youngest detrital-zircon ages being between 84 and 107 Ma (Albian–Santonian; Wu et al., 2010).

The Padana Formation, named after the Padana Valley south of Sangsang (Liu et al., 1988), is 733–2000 m thick and consists of varicolored sandstones interbedded with shales, minor conglomerates, and limestones. Best exposed in Sangsang, the unit conformably overlies the Ngamring Formation and is in fault contact with the Xigaze Ophiolite to the south. Its stratigraphic position indicates a Santonian–early Campanian age, consistent with youngest detrital-zircon ages between 78 and 84 Ma (Wu et al., 2010).

METHODS

Forty sandstone samples were selected for modal analysis (Fig. 3); over 400 points were counted on each sample, following the Gazzi-Dickinson method (Ingersoll et al., 1984). The results are presented in the supplementary material (GSA Data Repository, Table DR1 [see footnote 1]). Accessory minerals were separated by elutriation and magnetic separation from 13 sandstone samples selected from different sections. Five samples are from the lower Ngamring Formation (09QR07, 09NX09, 09NX15, 10AR13, 10AR-A15), three are from the middle Ngamring Formation (09NX34, 10AR25, 10AR-A08), two are from the upper Ngamring Formation (10AR02, 12AR07), and three are from the Padana Formation (09PDN-H, 09PDN01, 09PDN63). Zircon grains were handpicked, mounted in epoxy resin, and polished. U-Pb dating of detrital zircons was conducted by laser ablation–inductively coupled plasma–mass spectrometry (LA-ICP-MS) at the State Key Laboratory of Mineral Deposits Research, Nanjing University, following Jackson et al. (2004). To avoid grain-to-grain bias and to treat all samples equally, the laser spot was always placed in the core of the zircon grains; no cathodoluminescence (CL) imaging was performed. Various beam diameters (18–35 μm) were used, depending on the size of the zircon grains. The weighted $^{206}Pb/^{238}U$ age obtained of Mud Tank Zircon is 725.3 ± 4.7 Ma (n = 62), consistent with the predicted value (thermal ionization mass spectrometry [TIMS] age = 732 ± 5 Ma; Black and Gulson, 1978). GLITTER 4.4 was used for calculating results and relevant isotopic rates (Jackson et al., 2004). Age calculations and concordia diagrams were created using Isoplot 4.0 (Ludwig, 2011). Interpretations of zircon ages were based on $^{206}Pb/^{238}U$ ages for grains <1000 Ma and on $^{207}Pb/^{206}Pb$ ages for grains >1000 Ma. Zircons older than 200 Ma with discordance <10% and those younger than 200 Ma with discordance <20% were used. Dickinson and Gehrels (2009) concluded that weighted mean ages of two or more grain ages overlapping in age at 1σ (YC1σ[2+]) are more consistently compatible with depositional age, especially for strata derived from a contemporaneously active magmatic arc. Because sediments in the Xigaze forearc basin were mainly derived from the adjacent Gangdese arc, YC1σ(2+) ages could be used in this study to effectively constrain the maximum depositional ages of different units. U-Pb data are summarized in Table 1; the complete data set and sample locations are provided in the supplementary material (GSA Data Repository, Tables DR2 and DR7 [see footnote 1]).

In situ zircon Hf isotopic analyses were conducted on spots immediately adjacent to the locations used for the U-Pb age analysis. Hf isotopic compositions were determined with a Thermo Scientific Neptune Plus multicollector (MC) ICP-MS coupled to a New Wave UP193 solid-state laser-ablation system at the State Key Laboratory for Mineral Deposits Research, Nanjing University. Zircon grains were ablated with a beam diameter of 35 μm using an 8 Hz laser repetition rate or 25 μm with a 7 Hz laser repetition rate, and with energy of 15.5 J/cm^2. The Mud Tank standard was analyzed in every run, yielding $^{176}Hf/^{177}Hf = 0.282480 \pm 0.000031$ (2σ; n = 20), which is identical to the literature value of $^{176}Hf/^{177}Hf = 0.282522 \pm 0.000042$ (2σ; n = 2335) (Griffin et al., 2007). The complete data set is given in the supplementary material (GSA Data Repository, Table DR3 [see footnote 1]).

Thirteen samples of relatively fresh basalt collected at the base of the Chongdui Formation in the Naxia section (Fig. 2B) were powdered to <200 mesh for whole-rock analysis. Major elements were analyzed on an ARL9800XP+ spectrometer by X-ray fluorescence (XRF) in fused glass disks at the Centre of Materials Analysis, Nanjing University. Analytical precision is better than 5%. Trace elements were analyzed with an Agilent-7500a ICP-MS at State Key Laboratory of Marine Geology, Tongji University, Shanghai. Samples were dissolved with a mixture of HF and HNO_3 in Teflon digesting vessels on a hot plate for 24 h. This procedure was repeated using smaller amounts of acids for 12 h. After digestion, samples were dried, refluxed with 6 N HNO_3, and heated again to incipient dryness. Geological Standard Reference (GSR) materials were used to monitor analytical accuracy. Full results are given in the supplementary material (GSA Data Repository, Table DR4 [see footnote 1]).

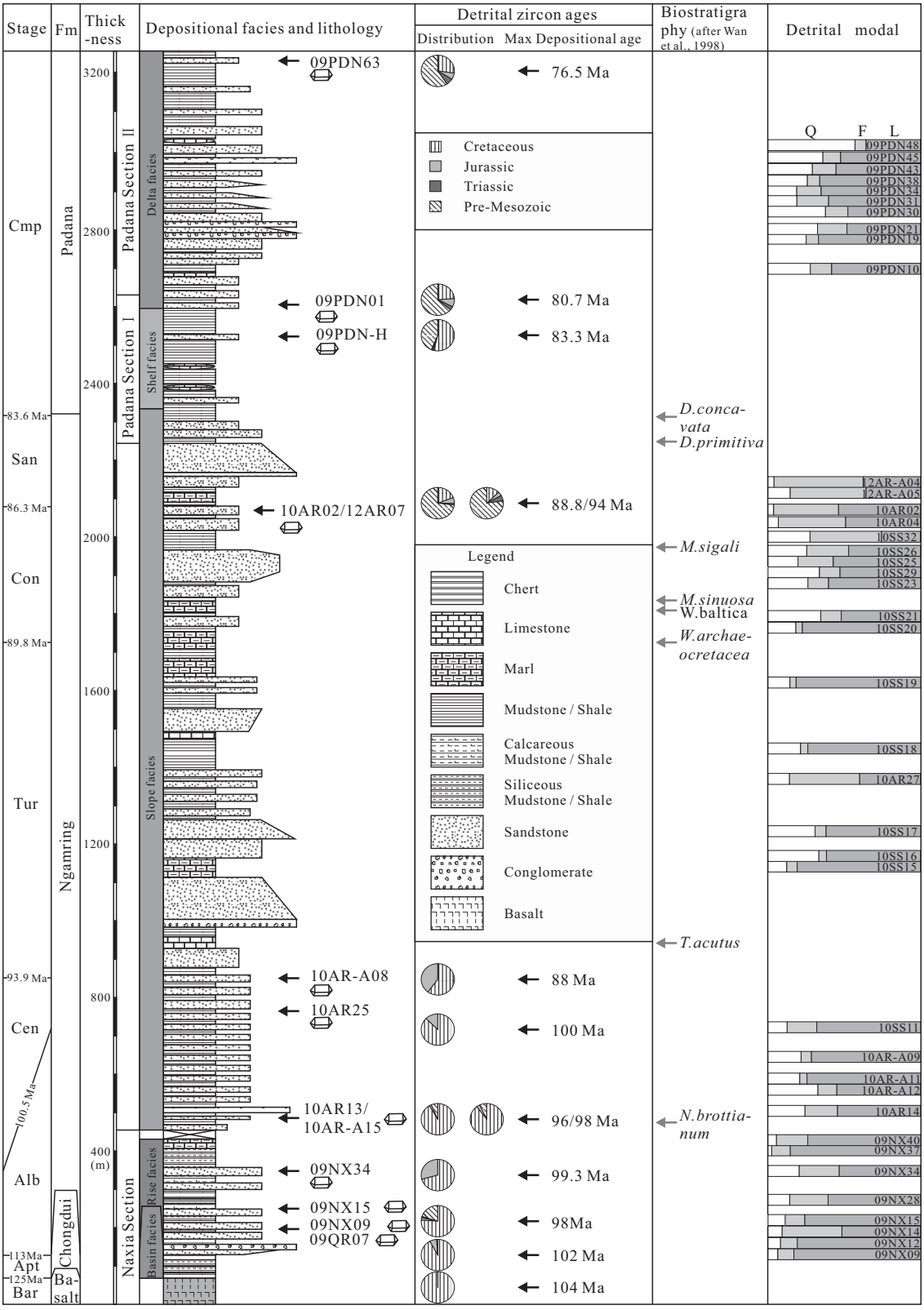

Figure 3. Diagram showing the stratigraphy of the Xigaze forearc basin with lithofacies, biostratigraphic data, age distribution, and maximum depositional age (YC1δ[2+] age; after Dickinson and Gehrels, 2009). Geological time scale is after Gradstein et al. (2012); biozones of the Ngamring Formation are after Wan et al. (1998). Cmp—Campanian; San—Santonian; Con—Coniacian; Tur—Turonian; Cen—Cenomanian; Alb—Albian; Apt—Aptian; Bar—Barremian; Q—quartz; F—feldspar; L—lithics; N.—*Neophlycticeras*; T.—*Turrilites*; W.—*Whiteinella*; M.—*Marginotruncana*; D.—*Dicarinella*.

TABLE 1. SUMMARIZED CHARACTERISTICS OF DETRITAL ZIRCON U-Pb AGES OF SANDSTONE SAMPLES FROM THE XIGAZE FOREARC BASIN

Formation	Sample	Analyzed numbers of zircon grains	Percentage of Mesozoic ages	Maximum depositional age* (Ma)	YDZ† (Ma)	YSG† (Ma)	YPP† (Ma)	YC1σ(2+)† (Ma)	YC2σ(3+)† (Ma)
Padana	09PDN63	*n* = 54	39% (21 out of 54)	76.5	74.9+2.3/–2.1	75 ± 2	74.9	76.5 ± 3.3 (*n* = 2)	80.2 ± 1.6 (*n* = 4)
	09PDN01	*n* = 78	35% (27 out of 78)	80.7	77.2+1.9/–2.4	77 ± 1	79.9	80.7 ± 1.2 (*n* = 3)	79.8 ± 1.0 (*n* = 4)
	09PDH-H	*n* = 69	51% (35 out of 69)	83.3	79.5+1.9/–4.2	80 ± 2	81.2	83.3 ± 0.9 (*n* = 9)	90.6 ± 0.6 (*n* = 24)
Upper Ngamring	10AR02	*n* = 61	28% (17 out of 61)	88.8	85.0+3.4/–5.7	86 ± 3	88.3	88.8 ± 1.8 (*n* = 6)	95.7 ± 1.4 (*n* = 12)
	12AR07	*n* = 69	20% (14 out of 69)	94	91.1+2.1/–2.3	74 ± 2	90.8	94 ± 4.2 (*n* = 2)	211.8 ± 3.4 (*n* = 4)
Middle Ngamring	10AR-A08	*n* = 57	100% (57 out of 57)	88	87.3+1.9/–1.9	88 ± 1	87.6	88 ± 1.0 (*n* = 2)	99.5 ± 0.8 (*n* = 24)
	10AR25	*n* = 59	100% (59 out of 59)	102.2	95.8+3.7/–15	95 ± 6	105.3	102.2 ± 2.3 (*n* = 11)	105.0 ± 1.5 (*n* = 24)
	09NX34	*n* = 80	100% (80 out of 80)	101.4	96.3+4.1/–7	98 ± 3	108.9	101.4 ± 2.2 (*n* = 7)	106.8 ± 1.0 (*n* = 24)
Lower Ngamring	10AR-A15	*n* = 56	93% (52 out of 56)	97.7	87+4.4/–4.4	87 ± 2	99.2	97.7 ± 1.0 (*n* = 13)	98.3 ± 0.8 (*n* = 24)
	10AR13	*n* = 46	96% (44 out of 46)	95.3	87.7+4/–4.3	80 ± 3	95.6	95.3 ± 1.4 (*n* = 11)	98.6 ± 1.0 (*n* = 24)
	09NX15	*n* = 67	81% (54 out of 67)	97.7	91.9+3.7/–14	93 ± 3	105.5	97.7 ± 1.8 (*n* = 11)	101.5 ± 1.2 (*n* = 24)
	09NX09	*n* = 84	99% (83 out of 84)	101.8	94.6+3.4/–8.8	96 ± 2	106	101.8 ± 1.6 (*n* = 13)	103.3 ± 1.3 (*n* = 24)
	09QR07	*n* = 59	100% (59 out of 59)	104.3	95.8+5/–11	101 ± 6	110	104.3 ± 2.2 (*n* = 13)	106.3 ± 1.5 (*n* = 24)

*Maximum depositional age is determined by YC1σ(2+).
†Different measures of youngest detrital zircon age after Dickinson and Gehrels (2009). YDZ—age calculated by the "youngest detrital zircon" routine of Isoplot (Ludwig, 2008); YSG—youngest single detrital zircon age with 1σ uncertainty; YPP—youngest graphical detrital zircon age peak on an age-probability plot or age-distribution curve; YC1σ(2+)—weighted mean age of two or more youngest grain ages overlapping in age at 1σ; YC2σ(3+)—weighted mean age of three or more youngest grain ages overlapping in age at 2σ.

RESULTS

New Data on Stratigraphy and Sedimentology of the Xigaze Forearc Basin

Our stratigraphic study was focused specifically on the Chongdui, Sangzugang, and Padana Formations (Figs. 2B, 2C, 3, 4, 5, and 6; Fig. DR1 [see footnote 1]).

Chongdui Formation

Based on our new detailed study of the completely exposed Naxia section southeast of Xigaze (Figs. 2A and 4), we here redefine the Chongdui Formation as the original lower chert member only, whereas the upper sandstone member is best considered as the lower part of the Ngamring Formation (megasequence 1[1] *in* Wang et al., 2012). In fact, the lithology, depositional environment, sandstone petrography, detrital-zircon U-Pb ages, and Hf isotopes of this newly defined lower part of the Ngamring Formation are the same as in the immediately overlying strata of the Ngamring Formation (Figs. 2A and 4). In depositional contact with the underlying basalt (Figs. 7A and 7B), the redefined Chongdui Formation is thus ~100 m thick, and it consists of centimeter-scale beds of purplish-greenish radiolarian chert dated at the late Barremian–late Aptian (Ziabrev et al., 2003), intercalated with greenish siliceous shale and dark-gray calcilutite (Fig. 8A). The Chongdui Formation is interpreted to have been deposited at abyssal depths on top of oceanic crust.

Sangzugang Formation

The Sangzugang Formation is in fault contact with either the Ngamring Formation or the Gangrinboche Conglomerate. It consists of grayish-black massive limestone with numerous calcite veins. Samples were taken every 5 m throughout the 45-m-thick section near Sangzugang village (Figs. A1 and A2 [see footnote 1]). Large agglutinated benthic foraminifera, small textulariids, and miliolids are most abundant in the lower part of the section, where *Cuneolina camposaurii*, *Nautiloculina oolithica*, *Mesorbitolina texana*, and *Palorbitolina discoidea* in sample 10SZG-C indicate a late Aptian age. Although foraminifera are rare and badly preserved through the rest of the unit, the presence of *Dictyoconus cuvillieri* from sample 10SZG-4 to the top of the section, where it occurs with *Mesorbitolina* sp., confirms a late Aptian to early Albian age (Boudagher-Fadel, 2008). The location of studied section, column, Microphotos for selected bethic foraminifera, locations and foraminiferal associations of samples related to the Sangzugang Formation are provided in the supplementary material (GSA Data Repository, Figs. DR1, DR2, DR3; Table DR8 [see footnote 1]).

Ngamring Formation

The ~270-m-thick upper part of the Naxia section, recognized as the lower part of the Ngamring Formation, is dominated by turbiditic sandstones commonly displaying flute, groove, and load casts, thinly interbedded with dark-gray calcareous and siliceous shales (Fig. 7D). At the base, debris-flow conglomerates contain pebbles of chert, limestone, basalt, and mudrock (Fig. 7C). Biostratigraphic data indicate that the Ngamring Formation was deposited during the late Albian to late Coniacian (100–86 Ma; Wan et al., 1998), consistent with the 107–84 Ma youngest peak ages of detrital zircons (Wu et al., 2010). Our five samples from the lower Ngamring Formation yielded YC1σ(2+) zircon ages of 104.3 ± 2.2, 101.8 ± 1.6, 97.7 ± 1.8, 95.3 ± 1.4, and 97.7 ± 1.0 Ma, respectively. Our three samples from the middle Ngamring Formation yielded YC1σ(2+) zircon ages of 101.4 ± 2.2, 102.2 ± 2.3, and 88 ± 1 Ma. Our two samples from the upper Ngamring Formation yielded YC1σ(2+) zircon ages of 94 ± 4.2 and 88.8 ± 1.8 Ma. The YC1σ(2+) zircon age at the base of the Padana Formation is 83.3 ± 0.9 Ma. We could thus constrain sedimentation in the lower, middle, and upper Ngamring Formation to have occurred between 104 and 99 Ma, between 99 and 88 Ma, and between 88 and 83 Ma, respectively.

Padana Formation

We investigated two sections in the Padana Valley south of Sangsang (Fig. 2C), in which three members were distinguished. Section I includes all of Member 1 from the top of the Ngamring Formation to the base of Member 2 (Fig. 5). Section II starts at the top of Member 1 (Fig. 6) and includes Members 2 and 3.

Member 1, ~370 m thick, consists of black shales and thin-bedded sandstones with minor limestones. Sandstone layers increase upward and locally display parallel lamination, bioturbation, and mud clasts. Deposition in shelf and prodelta environments is indicated.

Member 2, ~260 m thick, consists of varicolored siltstones and sandstones intercalated with black, greenish, and purple shales with calcareous concretions and burrows (Figs. 7E and 7F). Minor limestones, thin conglomerate beds containing pebbles of limestone and mudrock, and shelly beds with bivalves and gastropods also occur (Figs. 7G and 8E). Sandstones are arranged in upward-coarsening and thickening cycles and show graded bedding, parallel or oblique lamination (Fig. 7H), mud clasts and burrows, indicating deposition in distributary

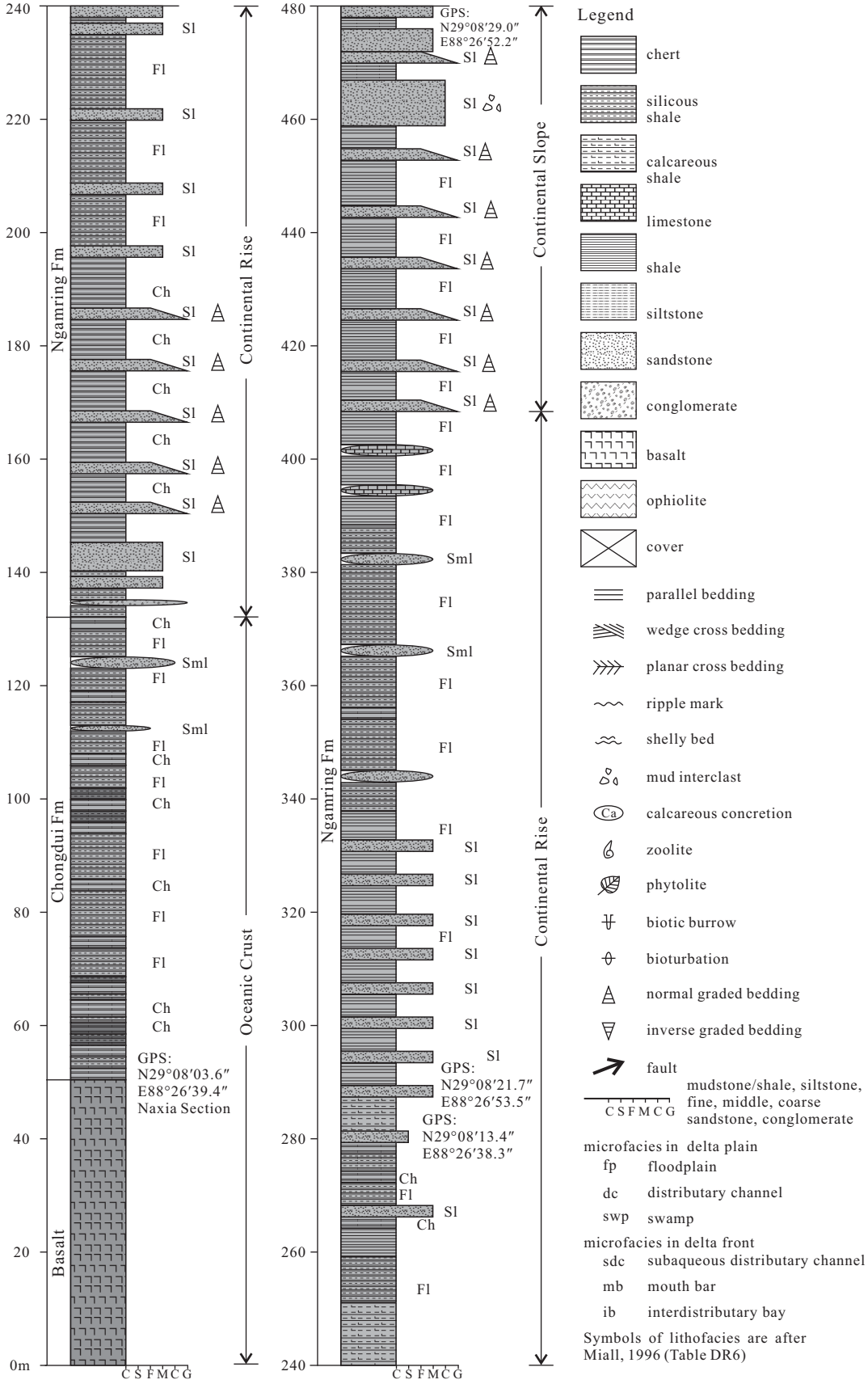

Figure 4. Stratigraphy of the Chongdui Formation in the Naxia section.

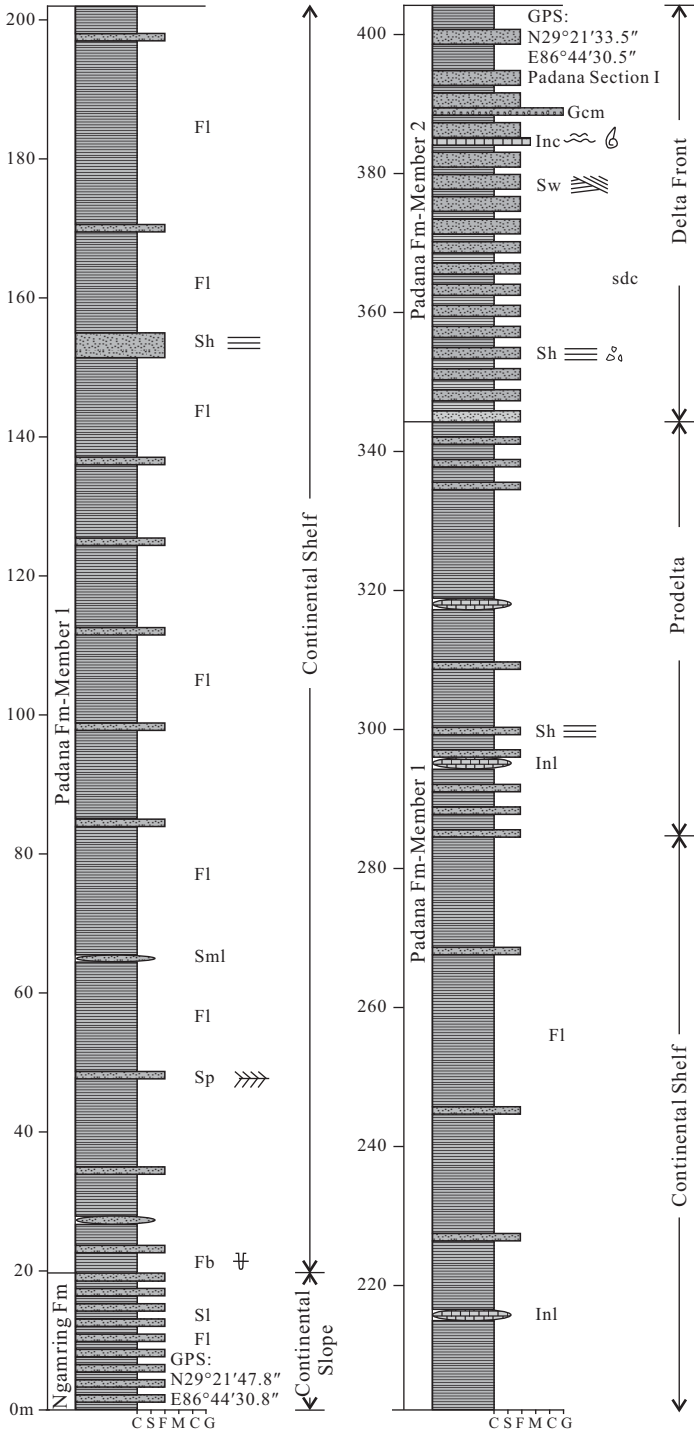

Figure 5. Stratigraphy of the Padana section I. Legend is the same as Figure 4.

channels to mouth-bar environments. Intercalated mudrocks represent interdistributary bay to floodplain deposits. Member 2 was deposited in delta-front to delta-plain environments at the top.

Member 3, ~380 m thick, consists of purple mudrock with pedogenetic calcareous concretions intercalated with thin-bedded sandstones with parallel lamination, burrows, and ripple marks. Deposition took place largely in subaerial delta-plain environments, including distributary channels and local swamps.

The depositional age of the Padana Formation is constrained between ca. 83 and ca. 76 Ma, as suggested by the two YC1σ(2+) zircon ages obtained from the lower part (83.3 ± 0.9 Ma, 80.7 ± 1.2 Ma) and by the YC1σ(2+) age obtained from the upper part (76.5 ± 3.3 Ma).

Provenance Analysis

Forearc-basin sandstones are generally derived from the adjacent magmatic arc (Dickinson and Seely, 1979). The classic provenance trend from "undissected" to "dissected magmatic arc" (Dickinson, 1985) is well documented in the upper Lower Cretaceous to Eocene strata of the Indus forearc basin in Ladakh (Garzanti and Van Haver, 1988; Garzanti et al., 1996). In this study, we conducted detailed petrographic analyses of the Ngamring and Padana Formations and integrated those results with U-Pb ages and Hf isotopic data on detrital zircons.

Sandstone Petrography

Ngamring sandstones are feldspatho-quartzo-lithic to quartzo-feldspatho-lithic volcaniclastic and plot in the "undissected" to "transitional" magmatic-arc provenance fields of Dickinson (1985) (average composition: quartz-feldspar-lithics [QFL] = 24:13:63 in the Ngamring-Sangsang areas; QFL = 10:30:60 in the Xigaze area; Figs. 8B, 8C, 8D, and 9A). Quartz grains are mainly monocrystalline and angular to subrounded. Plagioclase is only slightly more abundant than K-feldspar (Fig. 9B). Volcanic lithic fragments are dominantly microlitic and felsitic (Fig. 9C), with mafic lathwork types occurring at the base of the Ngamring Formation. Sedimentary lithic fragments include mudrock, limestone, and chert in the lower part of the unit.

Padana sandstones are mainly feldspatho-quartzo-lithic volcaniclastic and plot in the "transitional" to "dissected" magmatic arc or "recycled orogen" fields (average composition QFL = 31:14:55), suggesting upward-increasing contributions from intrusive rocks and possibly the recycling of older siliciclastic rocks (Figs. 8F and 9A). Subangular to rounded quartz grains are dominantly monocrystalline. K-feldspar prevails over plagioclase (Fig. 9B). Volcanic lithic fragments are mostly microlitic to felsitic; minor siltstone, mudrock, and limestone grains occur (Fig. 9C). Zircon, epidote, sphene, and biotite are the most common accessory minerals in both units.

Zircon U-Pb Ages and Hf Isotopes

Of the 312 usable ages obtained from the five lower Ngamring samples, 292 are Mesozoic (282 Cretaceous, with a main peak at 107 Ma; Fig. 10). The other 20 grains yielded ages older than 250 Ma. The youngest ages are 80 ± 3 Ma, 87 ± 2 Ma, and 88 ± 2 Ma, with discordances

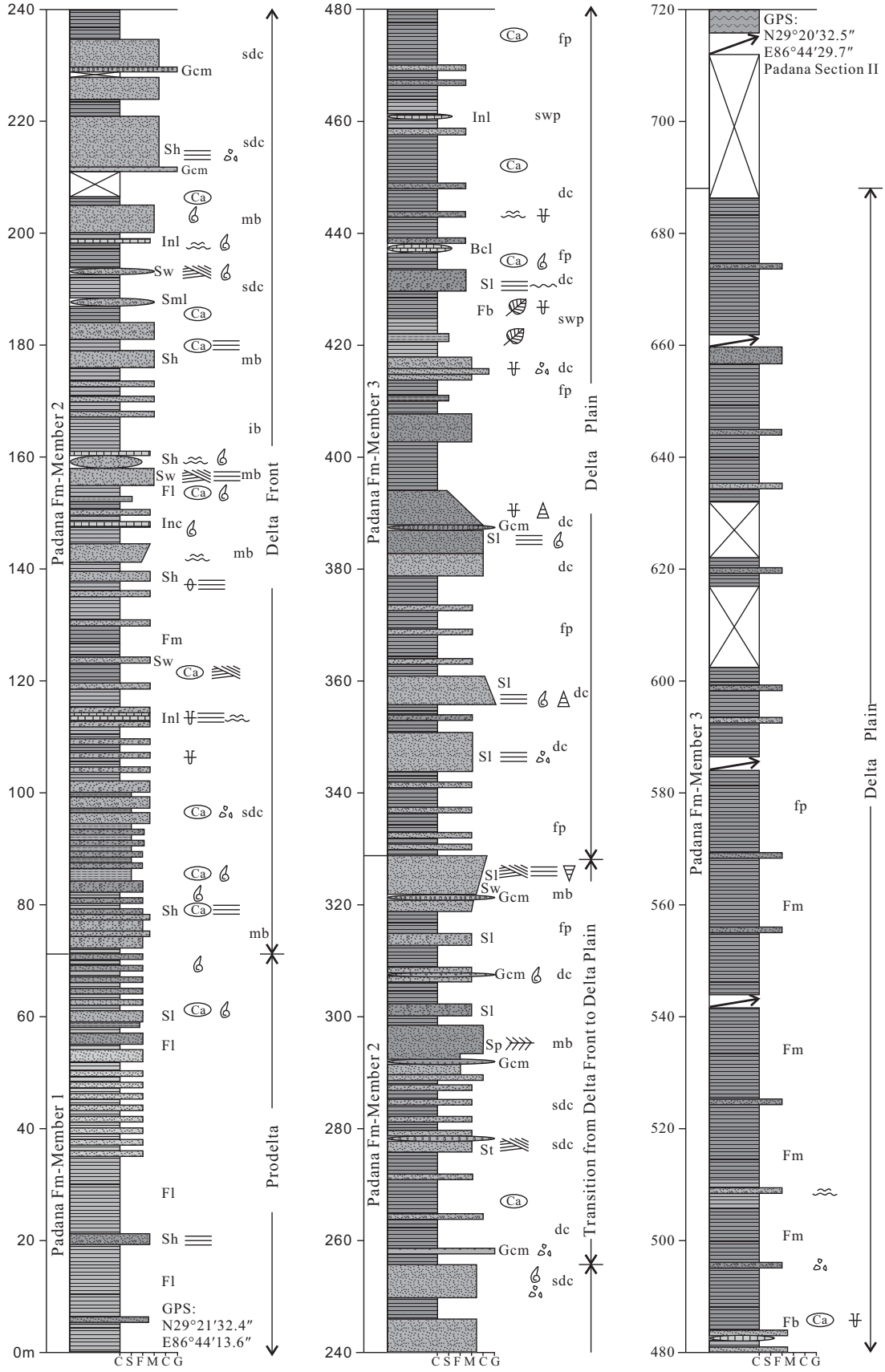

Figure 6. Stratigraphy of the Padana section II. Legend is the same as Figure 4.

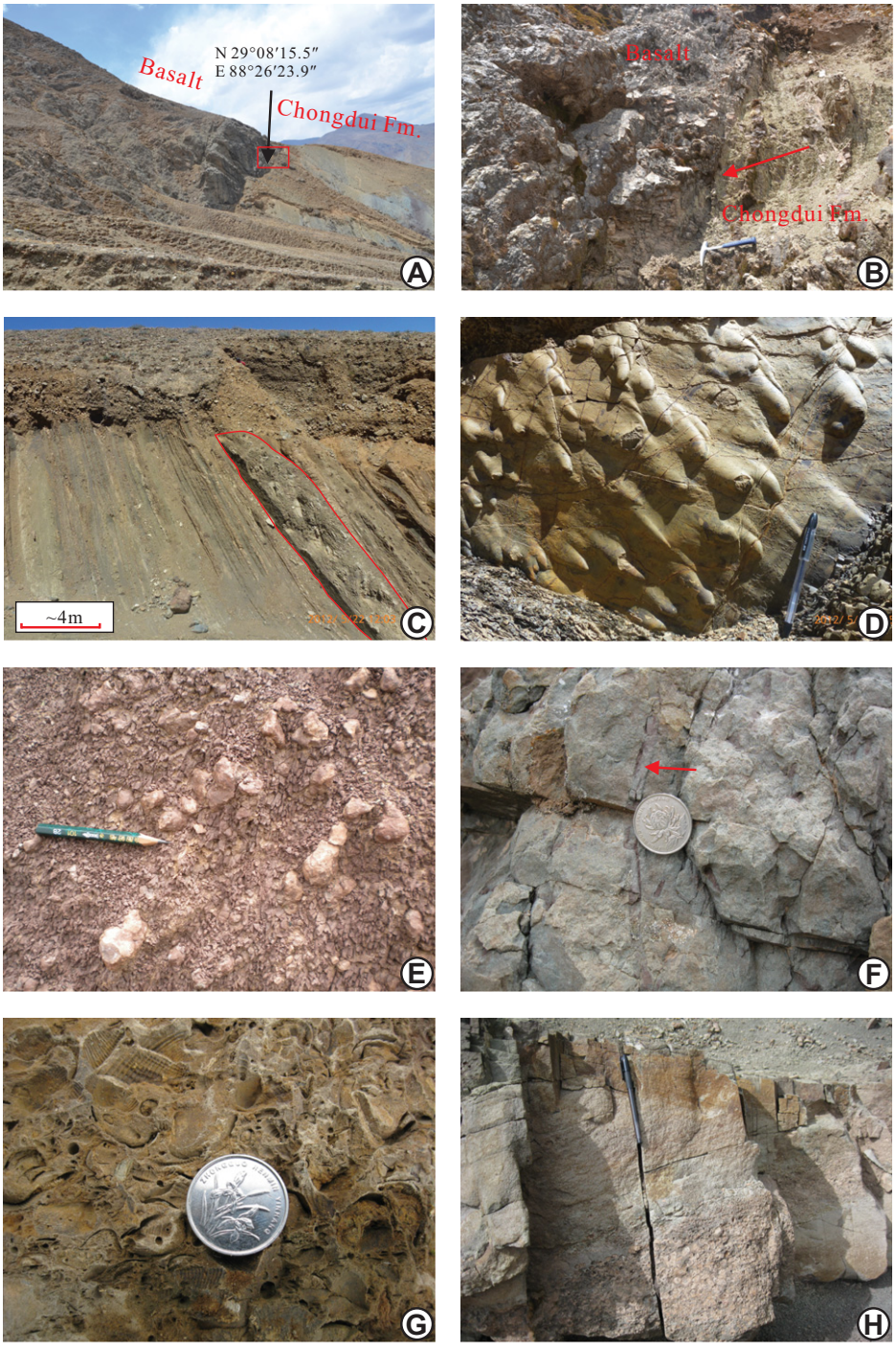

Figure 7. Main sedimentary structures in the Xigaze forearc-basin strata: (A–B) depositional contact between Xigaze forearc basalt and the overlying Chongdui Formation (Naxia section; rectangle in A is expanded in B; hammer for scale); (C) debris-flow conglomerate in the lower Ngamring Formation; (D) flute casts at the base of a Ngamring turbidite bed (pen for scale). Sedimentary structures in the Padana Formation: (E) pedogenic calcareous concretions; (F) burrows; (G) shell bed; (H) oblique lamination (coin, pen for scale).

of 2.5%, 11.5%, and –1.1%, respectively. Out of 33 Mesozoic grains, 32 show high $^{176}Hf/^{177}Hf$ ratios and positive $\varepsilon_{Hf(t)}$ values (from 0.282865 to 0.283137 and from 4.9 to 14.8, respectively).

All 196 concordant ages obtained from the three middle Ngamring samples are Mesozoic (144 Cretaceous, between 145 and 88 Ma, and 52 Jurassic, between 189 and 146 Ma; Fig. 10). The youngest ages are 88 ± 1 Ma, 88 ± 1 Ma, and 95 ± 6 Ma, with discordances of 4.5%, –3.4%, and 6.3%, respectively. The main age peaks are 100 Ma and 157 Ma. All 55 grains display high $^{176}Hf/^{177}Hf$ isotopic ratios and positive $\varepsilon_{Hf(t)}$ values (from 0.282855 to 0.283136, and from 5.2 to 14.7, respectively).

Among the 130 valid ages obtained from the two upper Ngamring samples, 31 are Mesozoic and 99 are older than 250 Ma (up to 3363 Ma). The youngest ages are 74 ± 2 Ma, 86 ± 3 Ma, and 87 ± 2 Ma, with discordances of 1.4%, 4.7%, and 1.1%, respectively. The age pattern is much more complex than for the lower and middle Ngamring Formation, with numerous small age clusters (at 1152, 586, 535, 216, 114, 101, 91, and 81 Ma). Thirty-one Mesozoic zircon grains show either high $^{176}Hf/^{177}Hf$ and positive $\varepsilon_{Hf(t)}$, or low $^{176}Hf/^{177}Hf$ and negative $\varepsilon_{Hf(t)}$ (from 0.281967 to 0.283065 and from –24.5 to 13.0, respectively).

The 201 ages obtained for the three Padana samples include 83 Mesozoic ages and 118 ages older than 250 Ma (up to 3114 Ma). The youngest ages are 75 ± 1 Ma, 77 ± 1 Ma, and 80 ± 1 Ma (2 grains), with discordances of 1.3%, 14.3%, 3.8%, and 3.5%, respectively. Similar to the upper Ngamring Formation, numerous small age clusters are present, and 68 Mesozoic zircons show either high $^{176}Hf/^{177}Hf$ and positive $\varepsilon_{Hf(t)}$ or low $^{176}Hf/^{177}Hf$ and negative $\varepsilon_{Hf(t)}$ values (from 0.282303 to 0.286072, and from –14.0 to 14.7, respectively).

Forearc Basalt

Grayish-green vesicular Naxia basalt of the Xigaze Ophiolite stratigraphically underlies the Chongdui Formation (Fig. 2B) and displays intergranular, diabasic, or ophitic texture. Elongate plagioclase laths are euhedral or subhedral, whereas pyroxene is altered to chlorite and epidote; carbonate replacements may be locally extensive (Figs. 8G and 8H).

Our samples have undergone various degrees of alteration, as indicated by petrographic observation and loss on ignition (LOI) ranging from 2.66 to 5.34 wt% and up to 7.2% in the most weathered sample. CaO and K_2O also vary widely (from 4.5 to 16.1 wt% and from 0.007 to 1.02 wt%, respectively). After normalizing major elements to 100% on an anhydrous basis,

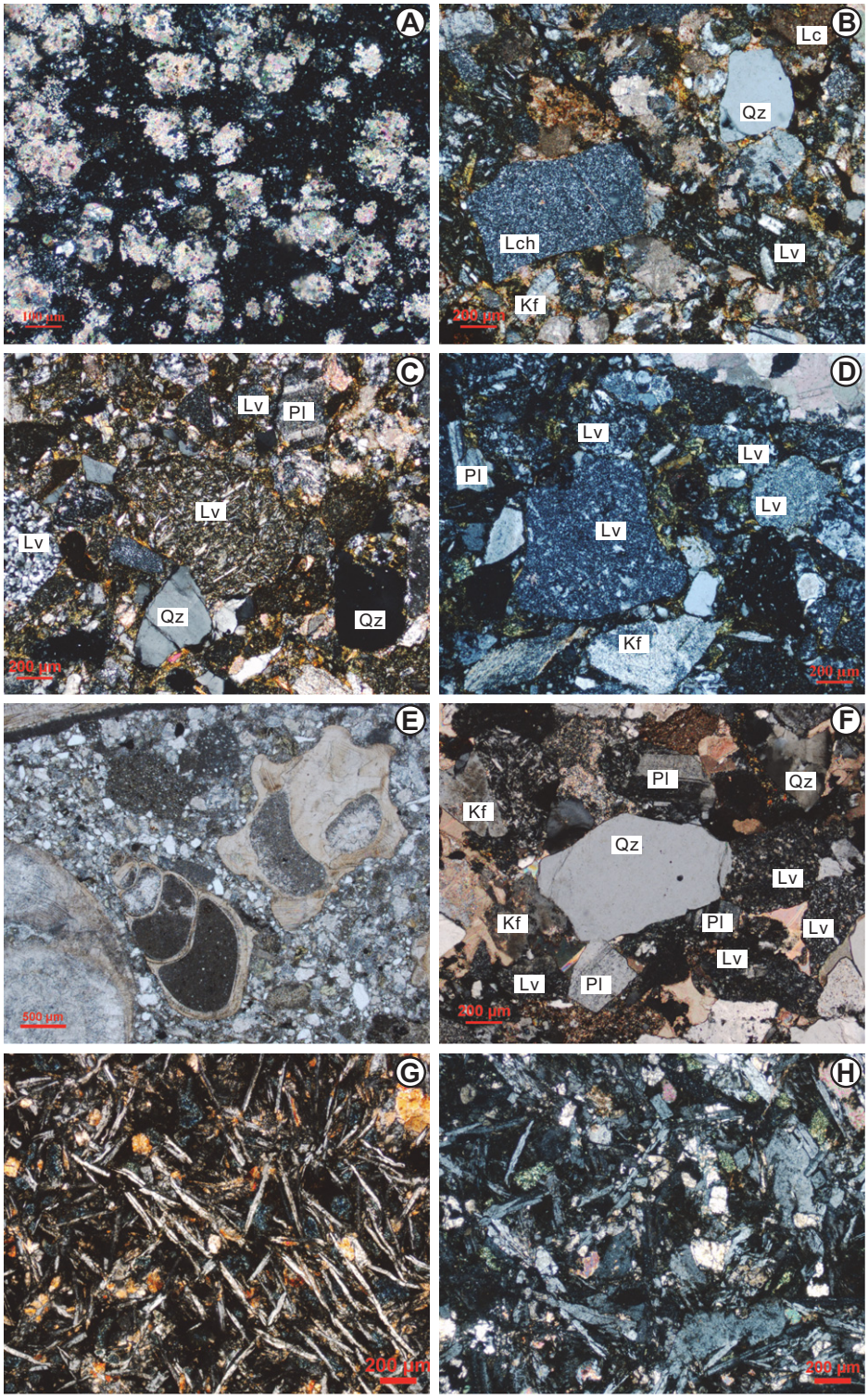

Figure 8. Microphotographs: (A) Chongdui chert with calcitized radiolaria (09NX06); (B) volcaniclastic sandstone with chert grains (upper Chongdui Formation; 09NX12); (C–D) volcaniclastic sandstones (Ngamring Formation; 10AR14, 10SS20); (E) quartzose wackestone with gastropods (Padana Formation; 09PDN20); (F) volcano-plutonic sandstone (Padana Formation; 09PDN39); (G–H) forearc basalt in the Naxia section (10WM01, 10WM02). Qz—quartz; Kf—K-feldspar; Pl—plagioclase; L—lithic fragments (Lm—metamorphic; Lv—volcanic; Lc—carbonate; Lch—chert).

ranges are SiO_2 from 49.0 to 55.2 wt% (average 52.5 wt%), $Na_2O + K_2O$ from 1.16 to 5.10 wt%, Al_2O_3 from 13.8 to 15.9 wt%, Fe_2O_3 from 10.4 to 14.9 wt%, TiO_2 from 1.1 to 2.1 wt%, and P_2O_5 from 0.08 to 0.16 wt%. Mg# [$100*Mg^{2+}/(Mg^{2+} + Fe^{2+})$] varies from 37 to 60 wt% (Table 2). Trace-element patterns show enrichment in large ion lithophile elements (LILEs: Cs, K, Sr, Ba) and in U and Hf (Fig. 11A). High Th in five samples may be due to alteration and was thus ignored in our interpretation. Chondrite-normalized rare earth element (REE) patterns (Sun and McDonough, 1989) show slight enrichment in heavy (H) REEs (Fig. 11B), no significant fractionation from light (L) REE to HREE (LREE/HREE = 1.3–1.6 and $[La/Yb]_N = 0.56–0.75$), and negligible Eu anomalies ($Eu/Eu^* = 0.86–1.18$).

The geochemistry of the Naxia basalt indicates normal mid-ocean-ridge basalt (N-MORB) affinity, consistent with previous studies on basalt of the Xigaze Ophiolite (Dai et al., 2013, and references therein). Most samples are classified as andesite/basalt on the Zr/TiO_2-Nb/Y diagram (Fig. 12A; Floyd and Winchester, 1978) and as MORB on the Ti-V diagram (Fig. 12B; Shervais, 1982). All samples plot as MORB, island-arc tholeiite basalt, or calc-alkali basalt on the Ti/100-Zr-3*Y diagram (Fig. 11C) and as N-MORB and volcanic arc basalt on the 2*Nb-Zr/4-Y diagram (Fig. 11D).

DISCUSSION

Petrofacies and Provenance Changes

Petrofacies

Sandstones from the Ngamring Formation to the Padana Formation display an upward increase in quartz at the expense of lithic fragments (Fig. 9A). Common limestone and chert fragments appear in the lower Ngamring Formation and decline in the middle and upper Ngamring and Padana units (Fig. 9C). Three distinct petrofacies (sensu Dickinson and Rich, 1972) can be identified in the Xigaze forearc-basin succession by integrating sandstone petrography and mineralogical data with detrital-zircon U-Pb ages and Hf isotopic signatures.

Petrofacies A (lower Ngamring Formation). Magmatic-arc provenance is testified by detrital modes (Fig. 9) and zircon grains with dominantly Mesozoic ages clustering at 107 Ma and positive $\varepsilon_{Hf(t)}$ (Fig. 10) (Cawood, 1991; Cawood et al., 2012). The minor pre-Mesozoic detrital zircons might have been derived from the arc basement now found locally in the eastern segment of the southern Lhasa subterrane (Zhu et al., 2013). A northern source from the Permian–Carboniferous strata of the central Lhasa subterrane is unlikely because the Gang-

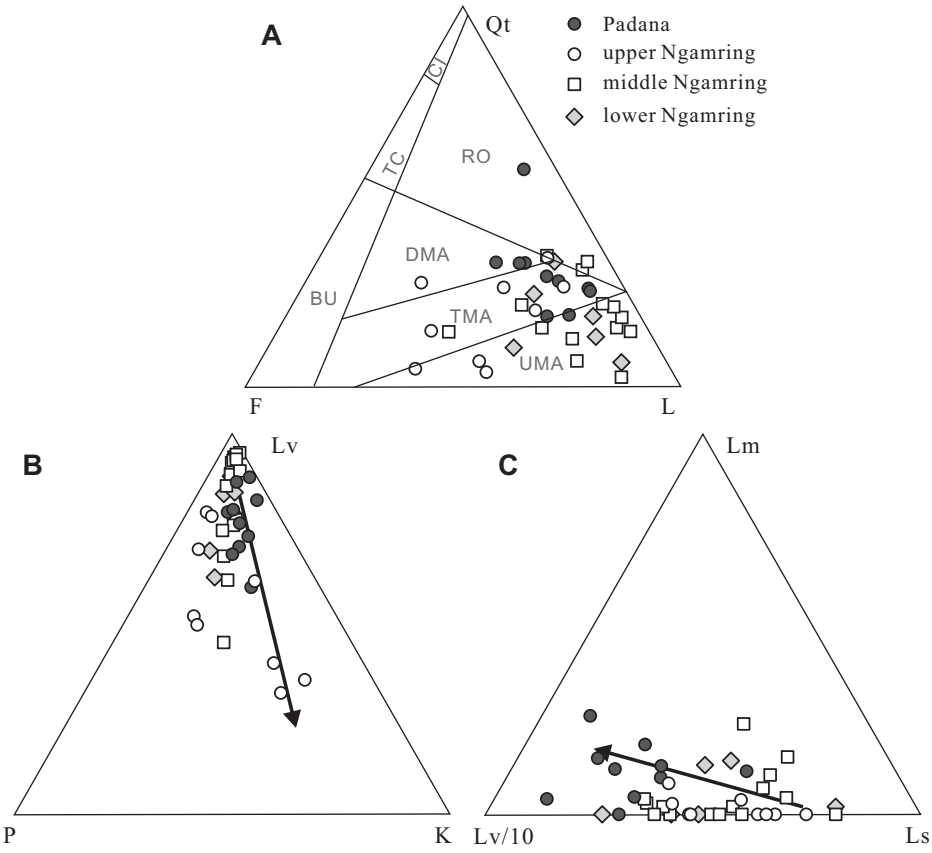

Figure 9. Triangular diagrams for Xigaze forearc-basin sandstones. (A) QtFL diagram after Dickinson (1985). (B) LvPK diagram. (C) LmLv/10Ls diagram. Qt—total quartz; F—feldspars (P—plagioclase; K—K-feldspar); L—lithic fragments (Lm—metamorphic; Lv/10—volcanic, divided by 10; Ls—sedimentary). Provenance fields after Dickinson (1985): RO—recycled orogenic; UMA—undissected magmatic arc; TMA—transitional magmatic arc; DMA—dissected magmatic arc; BU—basement uplift; TC—transitional continental; CI—craton interior.

dese arc had developed significant topography by ca. 105 Ma and at that time was providing detritus to the lower Takena Formation in the north (Leier et al., 2007). A xenocrystic/inherited source in Gangdese igneous rocks is also unlikely because similar older ages are not documented in the following petrofacies B when the Gangdese arc continued to supply sediments to the forearc basin. Detritus was thus derived dominantly from Lower Cretaceous magmatic rocks in the southern Gangdese arc, with minor supplies from older basement rocks and Sangzugang Formation, indicated by pre-Mesozoic detrital zircons and significant limestone clasts, respectively.

Petrofacies B (middle Ngamring Formation). Similar detrital modes and exclusively Mesozoic zircon ages with positive $\varepsilon_{Hf(t)}$ (Fig. 10) confirm magmatic-arc provenance. The appearance of an older zircon age peak at ca. 157 Ma with positive $\varepsilon_{Hf(t)}$ indicates an additional supply from older Jurassic magmatic rocks in the Gangdese arc (e.g., Yeba Formation and Sangri Group).

Petrofacies C (upper Ngamring and Padana Formations). The complex pattern of detrital-zircon U-Pb ages presents markedly more abundant pre-Mesozoic ages, numerous Mesozoic age clusters, and either positive $\varepsilon_{Hf(t)}$ or negative $\varepsilon_{Hf(t)}$ (Fig. 10). Abundant pre-Mesozoic detrital zircons were most likely derived from widespread Permian–Carboniferous metasedimentary rocks in the central Lhasa terrane. Provenance from the central Lhasa terrane is also indicated by Mesozoic zircons with negative $\varepsilon_{Hf(t)}$.

Causes of Provenance Change

Sandstone petrography, U-Pb ages, and Hf isotopes of detrital zircons are all consistent with the provenance of forearc-basin sandstones initially being from Lower Cretaceous Gangdese arc rocks, along with its basement and the Sangzugang Formation, next from Cretaceous and Jurassic Gangdese arc rocks, and finally from mixed sources in the Gangdese arc and central Lhasa terrane. A similar pattern of detrital-zircon ages observed in the Great Valley forearc basin of California was ascribed to a combination of broadening catchment areas associated with arc migration and widening of the arc-trench gap, changing shelf and submarine-canyon morphology, and progressive dissection of the magmatic arc (DeGraaff-Surpless et al., 2002). Because the entry points of detritus in the Xigaze forearc basin and their paleomorphology are unknown, we shall limit our discussion to the other two aspects.

The provenance change from petrofacies A to petrofacies B does not imply marked unroofing of the Gangdese arc, as detrital modes still plot in the "undissected" to "transitional" magmatic-arc field (Fig. 9A; Dickinson, 1985). The occurrence of zircon grains with Jurassic ages may thus be explained by expanding river catchments to also include older igneous rocks. The provenance change from petrofacies B to petrofacies C indicates more clearly that drainage areas increased further to include the central Lhasa terrane. River systems had to cut across the Gangdese arc to feed the forearc basin. A similar scenario was envisaged for the Rocky Mountain region in the mid-Eocene, with rivers passing the Cordilleran magmatic arc to reach the paleo–Pacific Ocean (Dickinson et al., 1988). The expansion of river catchments was fostered by uplift of the Lhasa terrane, which might have reached elevations of up to 3–4 km due to shortening and crustal thickening between 90 and 50 Ma (Murphy et al., 1997; Kapp et al., 2003, 2005, 2007), as supported by widespread Late Cretaceous magmatism possibly originated by lithospheric delamination (Zhao et al., 2008; Li et al., 2013; Yao et al., 2013; Liu et al., 2014; Wang et al., 2014). Uplift and erosion of the Lhasa terrane, also documented by a major hiatus spanning the Late Cretaceous to the Eocene in the southern Nima basin, resulted from collision with the Qiangtang block or reactivation of the Bangong suture (DeCelles et al., 2007).

ORIGIN OF THE XIGAZE OPHIOLITE

Extensive research has been conducted since the 1980s, when the Xigaze Ophiolite was thought to have formed at a slow-spreading ridge, based on the lack of large masses of cumulate gabbro and the presence of dolerite intrusives throughout the ophiolitic sequence (model 1, Fig. 13A; Nicolas et al., 1981; Girardeau et al., 1985a, 1985b; Girardeau and Mercier, 1988). Later on, new stratigraphic, mineral, and whole-

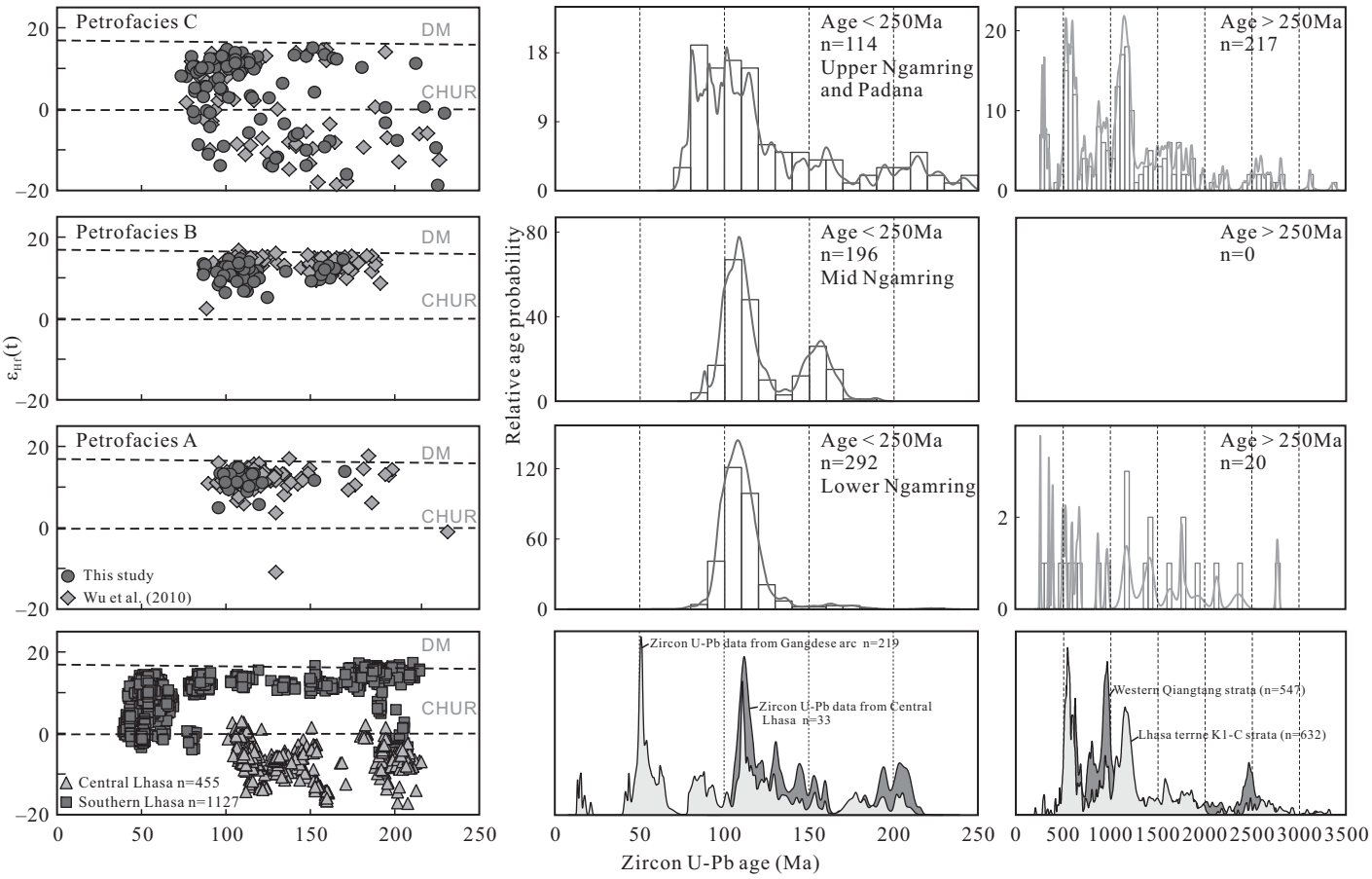

Figure 10. Age spectra and Hf isotopic signatures of detrital zircons (Hf data include results of Wu et al., 2010). Data from western Qiangtang (Zhu et al., 2011, and references therein), Lhasa terrane (Zhu et al., 2011, and references therein), and Gangdese arc (Ji et al., 2009, and references therein) are shown for comparison. DM—depleted mantle; CHUR—chondritic uniform reservoir.

rock geochemical data led researchers to suggest evolution in a complex back-arc system, with at least two intra-oceanic subduction zones active within the Neotethyan Ocean (model 2, Fig. 13B; Aitchison et al., 2000, 2003; Ziabrev et al., 2004; Hébert et al., 2003; Malpas et al., 2003; Dubois-Côté et al., 2005; Bédard et al., 2009; Bezard et al., 2011; Hébert et al., 2012). In this scenario, similar to what is envisaged for the Mesozoic arc-trench system of California (Ingersoll, 1982; Ingersoll and Schweickert, 1986; Dickinson et al., 1996), scraps of remnant-arc structures and older ophiolites should be found along the southern margin of the Lhasa terrane, and an unconformity should separate the Chongdui and Ngamring Formations.

Alternatively, the Xigaze Ophiolite may have formed by forearc spreading during the early stages of Neotethyan subduction (model 3, Fig. 13C; Dai et al., 2013). Forearc lithosphere and most ophiolites are in fact produced by

TABLE 2. SELECTED TRACE-ELEMENT CONCENTRATIONS AND RATIOS OF NAXIA BASALT IN THE NAXIA SECTION

			OIB	
	Naxia (average)	MORB	OIT	OIAB
Ba	4.18–26.26 (15.18)	5–50	70–200	200–1400
Sr	23.17–266.90 (151.89)	90–200	150–400	400–4000
Rb	0.18–8.20 (4.079)	<5	5–12	15–400
Zr	48.31–133.93 (90.73)	15–150	100–300	200–1000
Nb	0.77–1.66 (1.259)	1–15	5–25	20–60
Th/U	0.18–23.75 (4.192)	2	3–5	
Ce/Nb	7.05–8.60 (7.954)	3.85	17.8	
Zr/Nb	38.02–84.88 (72.356)	12–22	5.8	
Sr/Rb	29.68–212.2 (122.122)	127	20–70	
Th/Ta	1.1–31.67 (7.198)	0.75–2	N.D.*	
La/Ta	27.09–36.5 (32.986)	10–20	N.D.*	

Note: Reference data for mid-ocean-ridge basalt (MORB) and oceanic-island basalt (OIB) from Wilson (1989); OIT—oceanic-island tholeiite; OIAB—oceanic-island alkaline basalt. Trace elements are in ppm.
*N.D.—not determined.

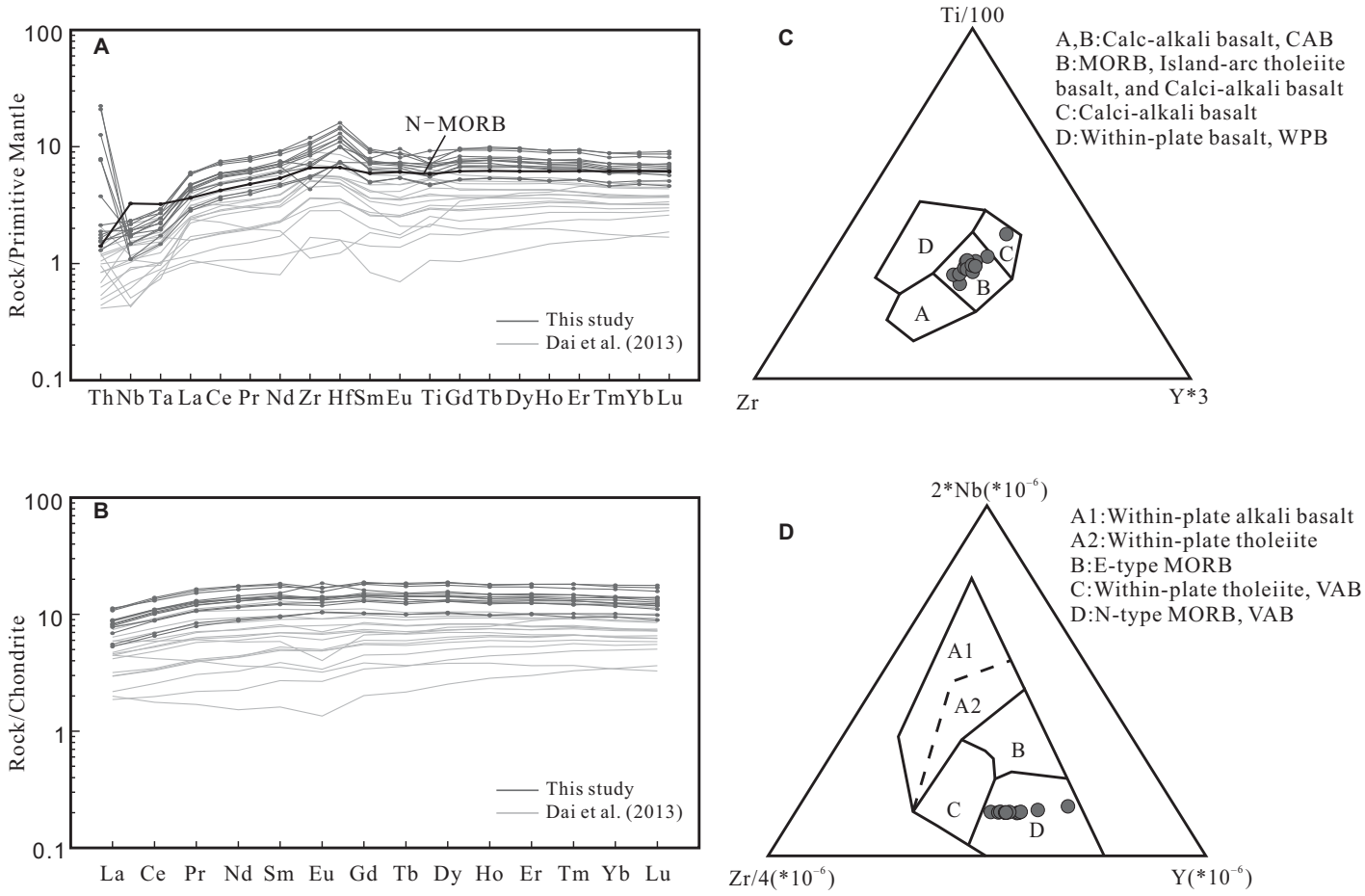

Figure 11. Discrimination diagrams showing the normal mid-ocean-ridge basalt (N-MORB) affinity of Xigaze forearc basalt. (A) Chondrite-normalized rare earth element (REE) patterns (after Taylor and McLennan, 1985); (B) N-MORB–normalized trace-element patterns (after Sun and McDonough, 1989); (C) Ti/100-Zr-Y*3 diagram (Pearce and Cann, 1973); and (D) 2*Nb-Zr/4-Y diagram (Meschede, 1986), where E type is enriched and N type is normal while VAB is volcanic arc basalt.

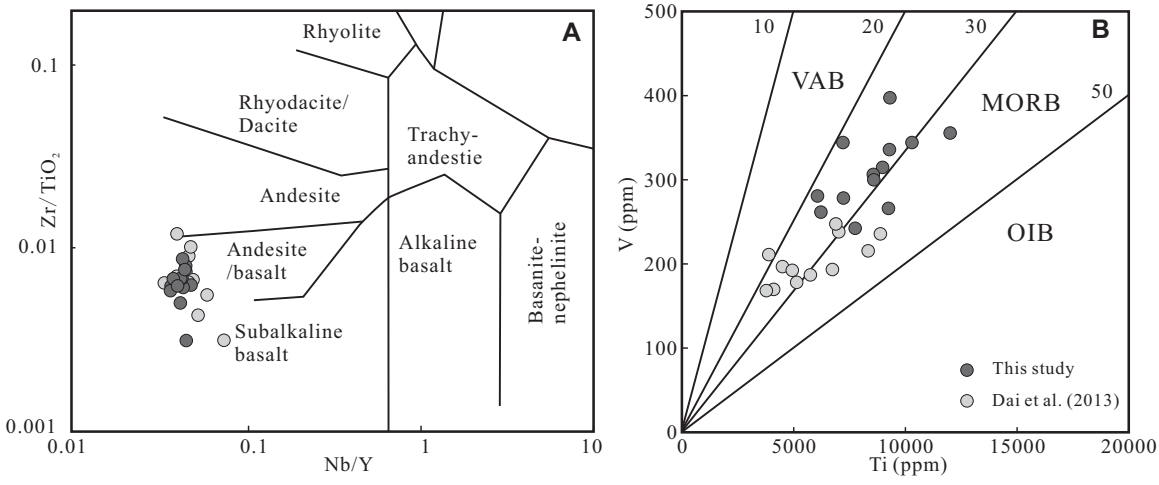

Figure 12. Geochemical plots for Xigaze forearc basalts: (A) Nb/Y-Zr/TiO_2 diagram (Floyd and Winchester, 1978); (B) Ti-V diagram (Shervais, 1982). VAB—volcanic arc basalt; MORB—mid-ocean-ridge basalt; OIB—oceanic-island basalt.

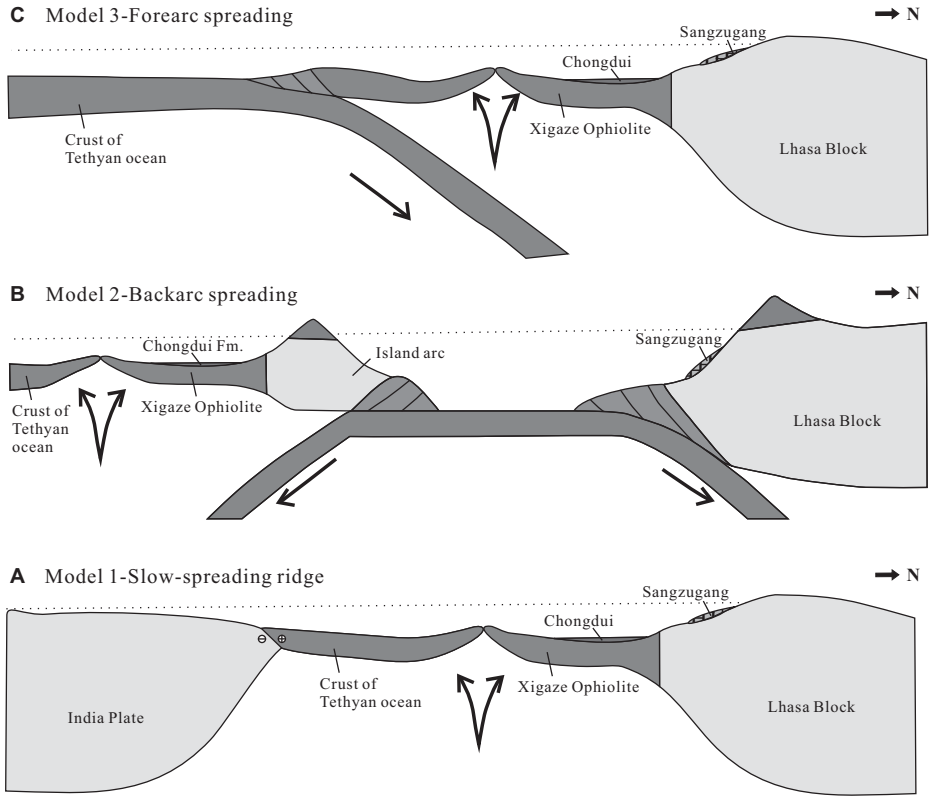

Figure 13. The three alternative models proposed for the tectonic setting of the Xigaze Ophiolite: (A) Girardeau et al. (1985a); (B) Hébert et al. (2012); and (C) Dai et al. (2013).

upwelling of metasomatized asthenosphere when subduction begins, and MORB-type lavas similar to those formed at mid-ocean ridges are generated (Stern, 2004; Whattam and Stern, 2011). This simpler scenario is consistent with all established geological and geochemical facts. The geochemical signatures of both peridotites and basalts indicate a suprasubduction origin (Pearce and Wanming, 1988; Dilek and Furnes, 2011; Hébert et al., 2012). The magmatic sequence (diorite, gabbro, diabase, basalt) has been dated with diverse methods at 130–123 Ma (Malpas et al., 2003; Wang et al., 2006; Dai et al., 2013; Zhang et al., 2013), corresponding well with the late Barremian–late Aptian biostratigraphic age of the overlying Chongdui Formation (127–117 Ma; Ziabrev et al., 2003). The Chongdui Formation stratigraphically overlies pillow basalts in several sections (e.g., Naxia and Qunrang, near Xigaze) (Bao and Wang, 1984; Wang and Liu, 1999; Ziabrev et al., 2003; Figs. 7A and 7B), and basaltic lava is intercalated with chert or encrusted by chert in the Naxia and Donglha sections (Ziabrev et al., 2003). The age and nature of its basal stratigraphic contact thus prove conclusively that the Chongdui chert was deposited on newly formed oceanic crust. The contact with turbidites of the overlying Ngamring Formation is also stratigraphic and conformable, demonstrating that the Naxia basalt and Chongdui chert represent the basement of the Xigaze forearc basin.

EVOLUTION OF THE XIGAZE FOREARC BASIN

The classic evolution of a forearc basin includes an early underfilled stage and a late filled stage, documented by an upward-shoaling sequence from deep-water turbidites to slope, shelfal, and eventually deltaic or even fluvial deposits (Dickinson and Seely, 1979; Ingersoll, 1982; Dickinson, 1995). This is matched perfectly by the Xigaze forearc-basin succession, deposited on an ophiolitic basement originated by forearc spreading and represented by abyssal cherts and turbidites of the Chongdui and Ngamring Formations (underfilled stage) passing upward to shelfal and fluvio-deltaic deposits of the Padana Formation (filled stage). Throughout the considered time, in association with the intermittent tectonic and topographic growth of the subduction complex, the basin evolved from a sloped stage (Chongdui Formation) to a ridged and terraced stage (Ngamring Formation), and finally to a shelved and benched stage (Padana Formation). Based on both sedimentological (Einsele et al., 1994; Wang et al., 2012) and provenance analysis, we identify five successive stages in the evolution of the Xigaze forearc basin.

(1) Late Barremian–Aptian (127–117 Ma): The Chongdui Formation records abyssal siliceous sedimentation during the sloped forearc-basin stage in the initial phases of Neotethyan subduction, when negligible sediment was produced because the nascent arc was still largely submerged. The upper Aptian to lower Albian Sangzugang Formation developed subsequently (117–110 Ma), on the shallow-marine northern edge of the Xigaze forearc basin.

(2) Albian–early Cenomanian (104–99 Ma): The lower Ngamring turbidites were deposited in deep-sea fan environments (megasequence 1[1] *in* Wang et al., 2012). The transition from the sloped stage to the ridged stage of forearc-basin sedimentation took place after the arc began to be actively eroded, and increasing volumes of arc-derived material were not only deposited in the forearc basin but also partly reached the trench, and then started to tectonically feed the growing subduction complex. Detritus was largely supplied by Lower Cretaceous magmatic rocks of the Gangdese arc, with minor contributions from its basement (as documented by the subordinate population of pre-Mesozoic zircons) and from erosion of the Sangzugang Formation (Fig. 14A).

(3) Cenomanian–early Coniacian (99–88 Ma): The middle Ngamring turbidites (megasequences 1[2] and 2 *in* Wang et al., 2012) were derived from both Cretaceous (ca. 100 Ma) and Jurassic (ca. 157 Ma) magmatic rocks of the Gangdese arc, and subordinately from the Sangzugang Formation (Fig. 14B). Precambrian zircons have not been found, and detrital modes do not indicate deep erosion of the active arc.

(4) Coniacian–Santonian (88–83 Ma): The upper Ngamring turbidites (megasequences 3–5 *in* Wang et al., 2012) were derived from both the Gangdese arc and the central Lhasa terrane (Fig. 14C). Uplift and erosion of the Lhasa terrane and expanding river catchments were presumably associated with increased sediment supply and the consequent progressive transition from the ridged to the terraced and finally shelved stages of forearc-basin sedimentation.

(5) Early Campanian (83–76 Ma): The Padana Formation records coastal to fluvio-deltaic sedimentation during the shelved to the benched stages of forearc-basin sedimentation, when the top of the continuously growing subduction complex reached sea level, and the forearc basin was eventually filled (Fig. 14D). Provenance of the detritus changed little, with a slight increase in quartz, possibly due in part to the recycling of older siliciclastic sediments.

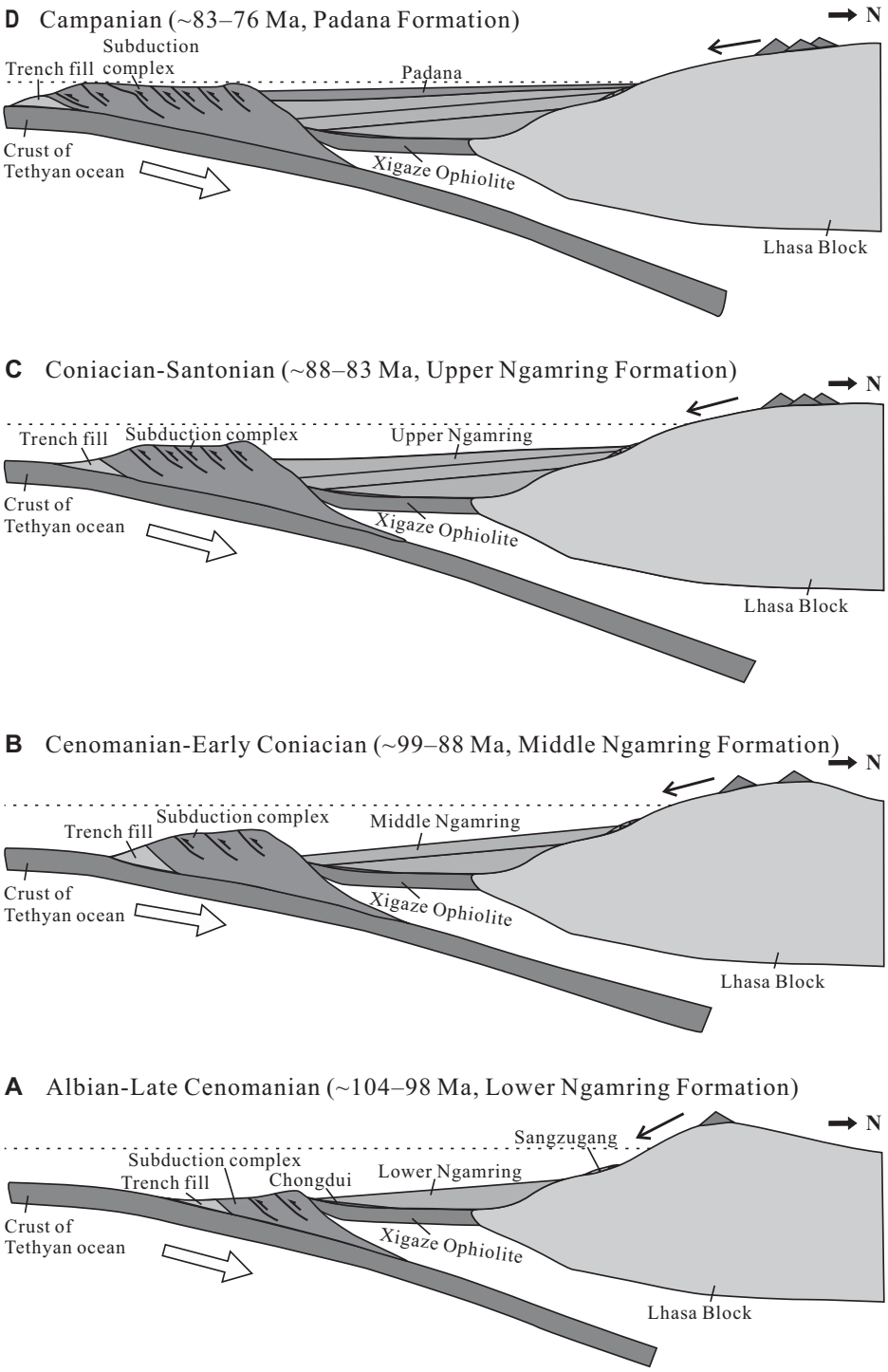

Figure 14. Schematic sections illustrating the envisaged evolution of the Xigaze forearc basin from Albian to Campanian times.

CONCLUSIONS

Our study reconstructs in detail the entire tectono-sedimentary history of the Xigaze forearc basin, ranging from the initial formation of oceanic crust during the initial subduction of Neotethyan oceanic lithosphere to the final filling by shelfal to fluvio-deltaic deposition. The upward-shallowing forearc-basin sequence provides a continuous record of magmatism, uplift, and exhumation of the Gangdese arc and central Lhasa terrane, allowing us to monitor the evolution of the Asian margin and uplift of the Tibetan Plateau during the Late Cretaceous.

In both the Xigaze and Indus forearc basins, deposition of rudistid reefs continued into the Albian (Sangzugang Formation in Tibet; Khalsi Limestone in Ladakh; Garzanti and Van Haver, 1988; Garzanti et al., 1996). Massive sand supply started with the Ngamring turbidites in the late Albian, possibly somewhat earlier than its counterpart in the west. Sandstone petrography, combined with detrital-zircon geochronology and geochemistry, allows us to recognize three sandstone petrofacies documenting the progressive erosional evolution of the Gangdese arc and Lhasa terrane. Volcanic and plutonic rocks of the Gangdese arc, along with their basement and Sangzugang carbonates, were eroded during mid-Cretaceous times (lower Ngamring Formation). In the Cenomanian–early Coniacian (middle Ngamring Formation), Jurassic magmatic rocks were also eroded, indicating the widening of river catchments to include larger areas within the Gangdese arc. The central Lhasa terrane was uplifted and eroded during Coniacian–Campanian times (upper Ngamring and Padana Formations). Based on sedimentological and provenance analysis, five stages are recognized during the evolution of the Xigaze forearc basin, represented by the Chongdui, lower Ngamring, middle Ngamring, upper Ngamring, and Padana Formations. The basement of the forearc sedimentary sequence is represented by the Xigaze Ophiolite, as documented by the stratigraphic contact between the abyssal cherts of the Chongdui Formation and the underlying pillow basalts.

ACKNOWLEDGMENTS

This work benefited from discussions with Lihui Chen, Fuyuan Wu, Chengshan Wang, Xianghui Li, Jingen Dai, and Dicheng Zhu. We thank Zhicheng Huang, Bin Wu, Zhifei Liu, and Anjun Lin for their assistance in the laboratory and Cong Wu, Hehe Jiang, Ronghua Guo, and Juan Li for their help in the field. This study was financially supported by the Ministry of Science and Technology of the People's Republic of China 973 Project (2012CB822001) and the Natural Science Foundation of China Project (41172092). Raymond Ingersoll and an anonymous reviewer, as well as Associate Editor Peter Cawood, provided greatly appreciated constructive comments.

REFERENCES CITED

Aitchison, J.C., Davis, A.M., Liu, J.B., Luo, H., Malpas, J.G., McDermid, I.R., Wu, H.Y., Ziabrev, S.V., and Zhou, M.F., 2000, Remnants of a Cretaceous intra-oceanic subduction system within the Yarlung–Zangbo suture (southern Tibet): Earth and Planetary Science Letters, v. 183, no. 1, p. 231–244, doi:10.1016/S0012-821X(00)00287-9.

Aitchison, J.C., Davis, A.M., Abrajevitch, A.V., Ali, J.R., Liu, J.B., Luo, H., McDermid, I.R., and Ziabrev, S.V., 2003, Stratigraphic and sedimentological constraints on the age and tectonic evolution of the Neotethyan ophiolites along the Yarlung Tsangpo suture zone,

Tibet, *in* Dilek, Y., and Robinson, R.T., eds., Ophiolites in Earth History: Geological Society of London Special Publication 218, p. 147–164, doi:10.1144/GSL.SP.2003.218.01.09.

Bao, P.C., and Wang, X.B., 1984, Geochemical Evidence for the Genesis of the Xigaze Ophiolite, Xizang (Tibet), Himalaya Geology: Beijing, Geological Publishing House, p. 59–82 (in Chinese with English abstract).

Bédard, É., Hébert, R., Guilmette, C., Lesage, G., Wang, C.S., and Dostal, J., 2009, Petrology and geochemistry of the Saga and Sangsang ophiolitic massifs, Yarlung Zangbo suture zone, southern Tibet: Evidence for an arc–back-arc origin: Lithos, v. 113, no. 1, p. 48–67, doi:10.1016/j.lithos.2009.01.011.

Bezard, R., Hébert, R., Wang, C., Dostal, J., Dai, J.G., and Zhong, H.T., 2011, Petrology and geochemistry of the Xiugugabu ophiolitic massif, western Yarlung Zangbo suture zone, Tibet: Lithos, v. 125, no. 1, p. 347–367, doi:10.1016/j.lithos.2011.02.019.

Black, L.P., and Gulson, B.L., 1978, The age of the Mud Tank carbonatite, Strangways Range, Northern Territory: BMR Journal of Australian Geology and Geophysics, v. 3, p. 227–232.

Boudagher-Fadel, M.K., 2008, Evolution and Geological Significance of Larger Benthic Foraminifera: Amsterdam, Elsevier, Developments in Paleontology and Stratigraphy, v. 21, 548 p.

Cai, F.L., Ding, L., Leary, R.J., Wang, H.Q., Xu, Q., Zhang, L.Y., and Yue, Y.H., 2012, Tectonostratigraphy and provenance of an accretionary complex within the Yarlung-Zangpo suture zone, southern Tibet: Insights into subduction-accretion processes in the Neo-Tethys: Tectonophysics, v. 574–575, p. 181–192, doi:10.1016/j.tecto.2012.08.016.

Cao, R.L., 1991, Sedimentology of trench-arc sediments and its relation to ophiolite obduction: Physics and Chemistry of the Earth, v. 18, p. 237–268, doi:10.1016/0079-1946(91)90003-X.

Cawood, P.A., 1983, Modal composition and detrital clinopyroxene geochemistry of lithic sandstones from the New England fold belt (east Australia): A Paleozoic forearc terrane: Geological Society of America Bulletin, v. 94, p. 1199–1214, doi:10.1130/0016-7606(1983)94<1199:MCADCG>2.0.CO;2.

Cawood, P.A., 1991, Characterization of intra-oceanic magmatic arc source terranes by provenance studies of derived sediments: New Zealand Journal of Geology and Geophysics, v. 34, p. 347–358, doi:10.1080/00288306.1991.9514473.

Cawood, P.A., 2005, Terra Australis orogen: Rodinia breakup and development of the Pacific and Iapetus margins of Gondwana during the Neoproterozoic and Paleozoic: Earth-Science Reviews, v. 69, p. 249–279, doi:10.1016/j.earscirev.2004.09.001.

Cawood, P.A., Leitch, E.C., Merle, R.E., and Nemchin, A.A., 2011, Orogenesis without collision: Stabilizing the Terra Australis accretionary orogen, eastern Australia: Geological Society of America Bulletin, v. 123, no. 11–12, p. 2240–2255, doi:10.1130/B30415.1.

Cawood, P.A., Hawkesworth, C., and Dhuime, B., 2012, Detrital zircon record and tectonic setting: Geology, v. 40, no. 10, p. 875–878, doi:10.1130/G32945.1.

Chu, M.F., Chung, S.L., Song, B., Liu, D., O'Reilly, S.Y., Pearson, N.J., Ji, J., and Wen, D.J., 2006, Zircon U-Pb and Hf isotope constraints on the Mesozoic tectonics and crustal evolution of southern Tibet: Geology, v. 34, no. 9, p. 745–748, doi:10.1130/G22725.1.

Dai, J.G., Wang, C.S., Hébert, R., Santosh, M., Li, Y.L., and Xu, J.Y., 2011a, Petrology and geochemistry of peridotites in the Zhongba ophiolite, Yarlung Zangbo suture zone: Implications for the Early Cretaceous intra-oceanic subduction zone within the Neo-Tethys: Chemical Geology, v. 288, no. 3–4, p. 133–148, doi:10.1016/j.chemgeo.2011.07.011.

Dai, J.G., Wang, C.S., Hébert, R., Li, Y.L., Zhong, H.T., Guillaume, R., Bezard, R., and Wei, Y.S., 2011b, Late Devonian OIB alkaline gabbro in the Yarlung Zangbo suture zone: Remnants of the Paleo-Tethys?: Gondwana Research, v. 19, no. 1, p. 232–243, doi:10.1016/j.gr.2010.05.015.

Dai, J.G., Wang, C.S., Polat, A., Santosh, M., Li, Y.L., and Ge, Y.K., 2013, Rapid forearc spreading between 130–120 Ma: Evidence from geochronology and geochemistry of the Xigaze Ophiolite, southern Tibet: Lithos, v. 172–173, p. 1–16, doi:10.1016/j.lithos.2013.03.011.

DeCelles, P.G., Kapp, P., Ding, L., and Gehrels, G., 2007, Late Cretaceous to middle Tertiary basin evolution in the central Tibetan Plateau: Changing environments in response to tectonic partitioning, aridification, and regional elevation gain: Geological Society of America Bulletin, v. 119, no. 5–6, p. 654–680, doi:10.1130/B26074.1.

DeGraaff-Surpless, K., Graham, S.A., Wooden, J.L., and McWilliams, M.O., 2002, Detrital zircon provenance analysis of the Great Valley Group, California: Evolution of an arc-forearc system: Geological Society of America Bulletin, v. 114, no. 12, p. 1564–1580, doi:10.1130/0016-7606(2002)114<1564:DZPAOT>2.0.CO;2.

Dickinson, W.R., 1985, Interpreting provenance relations from detrital modes of sandstones, *in* Zuffa, G.G., ed., Provenance of Arenites, NATO ASI Series Volume 148: Dordrecht, Netherlands, D. Reidel, p. 333–361.

Dickinson, W.R., 1995, Forearc basins, *in* Busby, C.J., and Ingersoll, R.V., eds., Tectonics of Sedimentary Basins: Cambridge, Massachusetts, Blackwell Science, p. 211–261.

Dickinson, W.R., and Gehrels, G.E., 2009, Use of U-Pb ages of detrital zircons to infer maximum depositional ages of strata: A test against a Colorado Plateau Mesozoic database: Earth and Planetary Science Letters, v. 288, no. 1, p. 115–125, doi:10.1016/j.epsl.2009.09.013.

Dickinson, W.R., and Rich, E.I., 1972, Petrologic intervals and petrofacies in the Great Valley Sequence, Sacramento Valley, California: Geological Society of America Bulletin, v. 83, p. 3007–3024, doi:10.1130/0016-7606(1972)83[3007:PIAPIT]2.0.CO;2.

Dickinson, W.R., and Seely, D., 1979, Structure and stratigraphy of forearc regions: American Association of Petroleum Geologists Bulletin, v. 63, no. 1, p. 2–31.

Dickinson, W.R., Klute, M.A., Hayes, M.J., Janecke, S.U., Lundin, E.R., McKittrick, M.A., and Olivares, M.D., 1988, Paleogeographic and paleotectonic setting of Laramide sedimentary basins in the central Rocky Mountain region: Geological Society of America Bulletin, v. 100, no. 7, p. 1023–1039, doi:10.1130/0016-7606(1988)100<1023:PAPSOL>2.3.CO;2.

Dickinson, W.R., Hopson, C.A., Saleeby, J.B., Schweickert, R., Ingersoll, R., Pessagno, E., Jr., Mattinson, J., Luyendyk, B., Beebe, W., and Hull, D., 1996, Alternate origins of the Coast Range ophiolite (California): Introduction and implications: GSA Today, v. 6, no. 2, p. 1–10.

Dilek, Y., and Furnes, H., 2011, Ophiolite genesis and global tectonics: Geochemical and tectonic fingerprinting of ancient oceanic lithosphere: Geological Society of America Bulletin, v. 123, no. 3–4, p. 387–411, doi:10.1130/B30446.1.

Ding, L., Kapp, P., and Wan, X., 2005, Paleocene–Eocene record of ophiolite obduction and initial India-Asia collision, south central Tibet: Tectonics, v. 24, no. 3, TC3001, doi:10.1029/2004TC001729.

Dong, H., Xu, F., Zeng, G., Wang, Q., Mao, Z., and Li, J., 2006, Is there a Neo-Tethys' subduction record earlier than arc volcanic rocks in the Sangri Group?: Acta Petrolei Sinica, v. 22, no. 3, p. 661–668.

Dubois-Côté, V., Hébert, R., Dupuis, C., Wang, C., Li, Y., and Dostal, J., 2005, Petrological and geochemical evidence for the origin of the Yarlung Zangbo ophiolites, southern Tibet: Chemical Geology, v. 214, no. 3, p. 265–286, doi:10.1016/j.chemgeo.2004.10.004.

Dürr, S.B., 1993, The mid to early Late Cretaceous Xigaze forearc basin (south Tibet): Sedimentary evolution and provenance of sediments [Ph.D. thesis]: Tübinger Geowissenschaftlische Arbeiten, Series A, v. 15, p. 119.

Dürr, S.B., 1996, Provenance of Xigaze fore-arc basin clastic rocks (Cretaceous, south Tibet): Geological Society of America Bulletin, v. 108, no. 6, p. 669–684, doi:10.1130/0016-7606(1996)108<0669:POXFAB>2.3.CO;2.

Einsele, G., Liu, B., Dürr, S., Frisch, W., Liu, G., Luterbacher, H., Ratschbacher, L., Ricken, W., Wendt, J., and Wetzel, A., 1994, The Xigaze forearc basin: Evolution and facies architecture (Cretaceous, Tibet): Sedimentary Geology, v. 90, no. 1, p. 1–32, doi:10.1016/0037-0738(94)90014-0.

Floyd, P., and Winchester, J., 1978, Identification and discrimination of altered and metamorphosed volcanic rocks using immobile elements: Chemical Geology, v. 21, no. 3, p. 291–306, doi:10.1016/0009-2541(78)90050-5.

Garzanti, E., and Van Haver, T., 1988, The Indus clastics: Forearc basin sedimentation in the Ladakh Himalaya (India): Sedimentary Geology, v. 59, no. 3, p. 237–249, doi:10.1016/0037-0738(88)90078-4.

Garzanti, E., Critelli, S., and Ingersoll, R.V., 1996, Paleogeographic and paleotectonic evolution of the Himalayan Range as reflected by detrital modes of Tertiary sandstones and modern sands (Indus transect, India and Pakistan): Geological Society of America Bulletin, v. 108, no. 6, p. 631–642, doi:10.1130/0016-7606(1996)108<0631:PAPEOT>2.3.CO;2.

Geng, Q., Pan, G.T., Wang, L., Zhu, D., and Liao, Z., 2006, Isotopic geochronology of the volcanic rocks from the Yeba Formation in the Gangdise zone, Xizang: Sedimentary Geology and Tethyan Geology, v. 26, no. 1, p. 1–7.

Girardeau, J., and Mercier, J., C., 1988, Petrology and texture of the ultramafic rocks of the Xigaze Ophiolite (Tibet): Constraints for mantle structure beneath slow-spreading ridges: Tectonophysics, v. 147, no. 1, p. 33–58.

Girardeau, J., Mercier, J., and Zhao, Y.G., 1985a, Origin of the Xigaze Ophiolite, Yarlung Zangbo suture zone, southern Tibet: Tectonophysics, v. 119, no. 1, p. 407–433, doi:10.1016/0040-1951(85)90048-4.

Girardeau, J., Mercier, J., and Zhao, Y.G., 1985b, Structure of the Xigaze Ophiolite, Yarlung Zangbo suture zone, southern Tibet, China: Genetic implications: Tectonics, v. 4, no. 3, p. 267–288, doi:10.1029/TC004i003p00267.

Göpel, C., Allègre, C.J., and Xu, R.H., 1984, Lead isotopic study of the Xigaze Ophiolite (Tibet): The problem of the relationship between magmatites (gabbros, dolerites, lavas) and tectonites (harzburgites): Earth and Planetary Science Letters, v. 69, no. 2, p. 301–310, doi:10.1016/0012-821X(84)90189-4.

Gradstein, F.M., Ogg, G., and Schmitz, M., 2012, The Geologic Time Scale: Boston, Massachusetts, Elsevier, 1176 p.

Griffin, W., Pearson, N., Belousova, E.A., and Saeed, A., 2007, Reply to "Comment to short-communication 'Comment: Hf-isotope heterogeneity in zircon 91500' by W.L., Griffin, N.J. Pearson, E.A. Belousova, and A. Saeed (Chemical Geology 233 [2006] 358–363)" by F. Corfu: Chemical Geology, v. 244, no. 1–2, p. 354–356, doi:10.1016/j.chemgeo.2007.06.023.

Hébert, R., Huot, F., Wang, C.S., and Liu, Z.F., 2003, Yarlung Zangbo ophiolites (southern Tibet) revisited: Geodynamic implications from the mineral record, *in* Dilek, Y., and Robinson, R.T., eds., Ophiolites in Earth History: Geological Society of London Special Publication 218, p. 165–190, doi:10.1144/GSL.SP.2003.218.01.10.

Hébert, R., Bezard, R., Guilmette, C., Dostal, J., Wang, C., and Liu, Z., 2012, The Indus–Yarlung Zangbo ophiolites from Nanga Parbat to Namche Barwa syntaxes, southern Tibet: First synthesis of petrology, geochemistry, and geochronology with incidences on geodynamic reconstructions of Neo-Tethys: Gondwana Research, v. 22, no. 2, p. 377–397, doi:10.1016/j.gr.2011.10.013.

Ingersoll, R.V., 1978, Petrofacies and petrologic evolution of the Late Cretaceous fore-arc basin, northern and central California: The Journal of Geology, v. 86, p. 335–352, doi:10.1086/649695.

Ingersoll, R.V., 1979, Evolution of the Late Cretaceous forearc basin, northern and central California: Geological Society of America Bulletin, v. 90, no. 9, p. 813–826, doi:10.1130/0016-7606(1979)90<813:EOTLCF>2.0.CO;2.

Ingersoll, R.V., 1982, Initiation and evolution of the Great Valley forearc basin of northern and central California, USA, *in* Leggett, J.K., ed., Trench-Forearc Geology: Sedimentation and Tectonics on Modern and Ancient Active Plate Margins: Geological Society of London

Special Publication 10, p. 459–467, doi:10.1144/GSL.SP.1982.010.01.31.
Ingersoll, R.V., 1983, Petrofacies and provenance of late Mesozoic forearc basin, northern and central California: American Association of Petroleum Geologists Bulletin, v. 67, no. 7, p. 1125–1142.
Ingersoll, R.V., 2012, Composition of modern sand and Cretaceous sandstone derived from the Sierra Nevada, California, USA, with implications for Cenozoic and Mesozoic uplift and dissection: Sedimentary Geology, v. 280, p. 195–207, doi:10.1016/j.sedgeo.2012.03.022.
Ingersoll, R.V., and Schweickert, R.A., 1986, A plate-tectonic model for Late Jurassic ophiolite genesis, Nevadan orogeny and forearc initiation, northern California: Tectonics, v. 5, no. 6, p. 901–912, doi:10.1029/TC005i006p00901.
Ingersoll, R.V., Fullard, T.F., Ford, R.L., Grimm, J.P., Pickle, J.D., and Sares, S.W., 1984, The effect of grain size on detrital modes; a test of the Gazzi-Dickinson point-counting method: Journal of Sedimentary Research, v. 54, no. 1, p. 103–116.
Jackson, S.E., Pearson, N.J., Griffin, W.L., and Belousova, E.A., 2004, The application of laser ablation–inductively coupled plasma–mass spectrometry to in situ U-Pb zircon geochronology: Chemical Geology, v. 211, no. 1, p. 47–69, doi:10.1016/j.chemgeo.2004.06.017.
Ji, W.Q., Wu, F.Y., Chung, S.L., Li, J.X., and Liu, C.Z., 2009, Zircon U-Pb geochronology and Hf isotopic constraints on petrogenesis of the Gangdese batholith, southern Tibet: Chemical Geology, v. 262, no. 3–4, p. 229–245, doi:10.1016/j.chemgeo.2009.01.020.
Kapp, P., Murphy, M.A., Yin, A., Harrison, T.M., Ding, L., and Guo, J., 2003, Mesozoic and Cenozoic tectonic evolution of the Shiquanhe area of western Tibet: Tectonics, v. 22, no. 4, doi:10.1029/2001TC001332.
Kapp, P., Yin, A., Harrison, T.M., and Ding, L., 2005, Cretaceous-Tertiary shortening, basin development, and volcanism in central Tibet: Geological Society of America Bulletin, v. 117, no. 7, p. 865–878, doi:10.1130/B25595.1.
Kapp, P., DeCelles, P., Leier, A., Fabijanic, J., He, S., Pullen, A., Gehrels, G., and Ding, L., 2007, The Gangdese retroarc thrust belt revealed: GSA Today, v. 17, no. 7, p. 4–9, doi:10.1130/GSAT01707A.1.
Leier, A.L., DeCelles, P.G., Kapp, P., and Ding, L., 2007, The Takena Formation of the Lhasa terrane, southern Tibet: The record of a Late Cretaceous retroarc foreland basin: Geological Society of America Bulletin, v. 119, no. 1–2, p. 31–48, doi:10.1130/B25974.1.
Li, J.G., Batten, D.J., and Zhang, Y.Y., 2008a, Late Cretaceous palynofloras from the southern Laurasian margin in the Xigaze region, Xizang (Tibet): Cretaceous Research, v. 29, no. 2, p. 294–300, doi:10.1016/j.cretres.2007.05.002.
Li, J.G., Batten, D.J., and Zhang, Y.Y., 2008b, Palynological indications of environmental changes during the Late Cretaceous–Eocene on the southern continental margin of Laurasia, Xizang (Tibet): Palaeogeography, Palaeoclimatology, Palaeoecology, v. 265, no. 1–2, p. 78–86.
Li, Y.L., He, J., Wang, C.S., Santosh, M., Dai, J.G., Zhang, Y.X., Wei, Y.S., and Wang, J.G., 2013, Late Cretaceous K-rich magmatism in central Tibet: Evidence for early elevation of the Tibetan Plateau?: Lithos, v. 160, p. 1–13, doi:10.1016/j.lithos.2012.11.019.
Liu, C.J., Yin, J.X., Sun, X.X., and Sun, Y.Y., 1988, Marine Late Cretaceous–Early Tertiary sequences: The non-flysch deposits of the Xigaze forearc basin in south Xizang: Memoirs of Institute of Geology, Academia Sinica, v. 3, p. 130–157 (in Chinese).
Liu, D., Zhao, Z.D., Zhu, D.C., Niu, Y.L., and Harrison, T.M., 2014, Zircon xenocrysts in Tibetan ultrapotassic magmas: Imaging the deep crust through time: Geology, v. 42, no. 1, p. 43–46, doi:10.1130/G34902.1.
Ludwig, K.R., 2011, Isoplot/Ex Version 4: A Geochronological Toolkit for Microsoft Excel: Berkeley Geochronology Center Special Publication 4, 70 p.
Malpas, J., Zhou, M.F., Robinson, P.T., and Reynolds, P.H., 2003, Geochemical and geochronological constraints on the origin and emplacement of the Yarlung Zangbo ophiolites, southern Tibet, *in* Dilek, Y., and Robinson, R.T., eds., Ophiolites in Earth History: Geological Society of London Special Publication 218, p. 191–206, doi:10.1144/GSL.SP.2003.218.01.11.
Meschede, M., 1986, A method of discriminating between different types of mid-ocean ridge basalts and continental tholeiites with the Nb*2-Zr/4-Y diagram: Chemical Geology, v. 56, no. 3, p. 207–218, doi:10.1016/0009-2541(86)90004-5.
Miall, A.D., 1996, The Geology of Fluvial Deposits: Berlin, Springer, 582 p.
Murphy, M., Yin, A., Harrison, T., Dürr, S., Chen, Z., Ryerson, F., Kidd, W., Wang, X., and Zhou, X., 1997, Did the Indo-Asian collision alone create the Tibetan Plateau?: Geology, v. 25, no. 8, p. 719–722, doi:10.1130/0091-7613(1997)025<0719:DTIACA>2.3.CO;2.
Nicolas, A., Girardeau, J., Marcoux, J., Dupre, B., Wang, X.B., Cao, Y.G., Zheng, H.X., and Xiao, X.C., 1981, The Xigaze Ophiolite (Tibet): A peculiar oceanic lithosphere: Nature, v. 294, p. 414–417, doi:10.1038/294414a0.
Pan, G.T., Ding, J., Yao, D., and Wang, L., 2004, The Guide Book of Geologic Map of the Qinghai-Xizang (Tibet) Plateau and Adjacent Areas: Chengdu, Chengdu Cartographic Publishing House, scale 1:1,500,000 (in Chinese with English abstract).
Pan, G.T., Mo, X.X., Hou, Z.Q., Zhu, D.C., Wang, L.Q., Li, G.M., Zhao, Z.D., Geng, Q.R., and Liao, Z.L., 2006, Spatial-temporal framework of the Gangdese orogenic belt and its evolution: Acta Petrolei Sinica, v. 22, no. 3, p. 521–533.
Pearce, J., and Cann, J., 1973, Tectonic setting of basic volcanic rocks determined using trace element analyses: Earth and Planetary Science Letters, v. 19, no. 2, p. 290–300, doi:10.1016/0012-821X(73)90129-5.
Pearce, J.A., and Wanming, D., 1988, The ophiolites of the Tibetan geotraverses, Lhasa to Golmud (1985) and Lhasa to Kathmandu (1986): Philosophical Transactions of the Royal Society of London, ser. A, Mathematical and Physical Sciences, v. 327, no. 1594, p. 215–238, doi:10.1098/rsta.1988.0127.
Shervais, J.W., 1982, Ti-V plots and the petrogenesis of modern and ophiolitic lavas: Earth and Planetary Science Letters, v. 59, no. 1, p. 101–118, doi:10.1016/0012-821X(82)90120-0.
Stern, R.J., 2004, Subduction initiation: Spontaneous and induced: Earth and Planetary Science Letters, v. 226, no. 3–4, p. 275–292, doi:10.1016/j.epsl.2004.08.007.
Sun, S.S., and McDonough, W.F., 1989, Chemical and isotopic systematics of oceanic basalts: Implications for mantle composition and processes, *in* Saunders, A.D., and Norry, M.J., eds., Magmatism in the Ocean Basins: Geological Society of London Special Publication 42, p. 313–345, doi:10.1144/GSL.SP.1989.042.01.19.
Taylor, S.R., and McLennan, S.M., 1985, The Continental Crust: Its Composition and Evolution: London, Blackwell, Oxford, 312 p.
Wan, X.Q., Wang, C.S., and Wang, L., 1997, Discovery of Cretaceous foraminifera in the Xigaze forearc basin, Xizang—With a chronostratigraphic discussion: Acta Geologica Sinica, v. 71, no. 3, p. 193–201.
Wan, X.Q., Wang, L., Wang, C.S., and Jansa, L., 1998, Discovery and significance of Cretaceous fossils from the Xigaze forearc basin, Tibet: Journal of Asian Earth Sciences, v. 16, no. 2, p. 217–224.
Wang, C.S., and Liu, Z.F., 1999, Xigaze Forearc Basin and Yarlung Zangbo Suture Zone, Tibet: Beijing, Geological Publishing House, p. 1–237 (in Chinese with English abstract).
Wang, C.S., Li, X.H., Liu, Z.F., Li, Y.L., Jansa, L., Dai, J.G., and Wei, Y.S., 2012, Revision of the Cretaceous–Paleogene stratigraphic framework, facies architecture and provenance of the Xigaze forearc basin along the Yarlung Zangbo suture zone: Gondwana Research, v. 22, no. 2, p. 415–433, doi:10.1016/j.gr.2011.09.014.
Wang, J.G., Hu, X.M., Wu, F.Y., and Jansa, L., 2010, Provenance of the Liuqu Conglomerate in southern Tibet: A Paleogene erosional record of the Himalayan–Tibetan orogen: Sedimentary Geology, v. 231, no. 3–4, p. 74–84, doi:10.1016/j.sedgeo.2010.09.004.
Wang, J.G., Hu, X.M., Garzanti, E., and Wu, F.Y., 2013, Upper Oligocene–Lower Miocene Gangrinboche Conglomerate in the Xigaze area, southern Tibet: Implications for Himalayan uplift and paleo–Yarlung-Zangbo initiation: The Journal of Geology, v. 121, no. 4, p. 425–444, doi:10.1086/670722.
Wang, Q., Zhu, D.C., Zhao, Z.D., Liu, S.A., Chung, S.L., Li, S.M., Liu, D., Dai, J.G., Wang, L.Q., and Mo, X.X., 2014, Origin of the ca. 90 Ma magnesia-rich volcanic rocks in the SW Nyima, central Tibet: Products of lithospheric delamination beneath the Lhasa-Qiangtang collision zone: Lithos, v. 198–199, p. 24–37, doi:10.1016/j.lithos.2014.03.019.
Wang, R., Xia, B., Zhou, G., Zhang, Y., Yang, Z., Li, W., Wei, D., Zhong, L., and Xu, L., 2006, SHRIMP zircon U-Pb dating for gabbro from the Tiding ophiolite in Tibet: Chinese Science Bulletin, v. 51, p. 1776–1779, doi:10.1007/s11434-006-2027-y.
Wen, D.R., Liu, D.Y., Chung, S.L., Chu, M.F., Ji, J.Q., Zhang, Q., Song, B., Lee, T.Y., Yeh, M.W., and Lo, C.H., 2008, Zircon SHRIMP U-Pb ages of the Gangdese Batholith and implications for Neotethyan subduction in southern Tibet: Chemical Geology, v. 252, no. 3, p. 191–201, doi:10.1016/j.chemgeo.2008.03.003.
Wen, S.X., 1974, The Cretaceous and Tertiary System. A Report of the Scientific Expedition in the Mount Qomolangma Region (1966–1968): Beijing, Science Press, p. 148–212 (in Chinese with English abstract).
Whattam, S.A., and Stern, R.J., 2011, The 'subduction initiation rule': A key for linking ophiolites, intra-oceanic forearcs, and subduction initiation: Contributions to Mineralogy and Petrology, v. 162, no. 5, p. 1031–1045, doi:10.1007/s00410-011-0638-z.
Wilson, B.M., 1989, Igneous Petrogenesis: A Global Tectonic Approach: London, Chapman & Hall, 466 p.
Wu, F.Y., Ji, W.Q., Liu, C.Z., and Chung, S.L., 2010, Detrital zircon U-Pb and Hf isotopic data from the Xigaze fore-arc basin: Constraints on Transhimalayan magmatic evolution in southern Tibet: Chemical Geology, v. 271, no. 1–2, p. 13–25, doi:10.1016/j.chemgeo.2009.12.007.
Wu, H.R., 1984, The deep-sea sedimentary strata in southern Tibet—The Chongdoi Formation and its geological significance: Geosciences, v. 1, p. 26–35.
Wu, H.R., Wang, D.A., and Wang, L.C., 1977, The Cretaceous of Laze-Jiangze district, Southern Xizang: Scientia Geologica Sinica, v. 3, p. 250–261.
Xia, B., Yu, H.X., Chen, G.W., Qi, L., Zhao, T.P., and Zhou, M.F., 2003, Geochemistry and tectonic environment of the Dagzhuka ophiolite in the Yarlung-Zangbo suture zone, Tibet: Geochemical Journal, v. 37, no. 3, p. 311–324, doi:10.2343/geochemj.37.311.
Xiao, X.C., 1984, The Xigaze Ophiolite of Southern Tibet and its Relevant Tectonic Problems: Sino–French Cooperative Investigation in Himalayas: Beijing, Geological Publishing House, p. 143–168 (in Chinese with English abstract).
Xizang Bureau of Geology and Mineral Resources (XBGMR), 1997, Regional Lithostrata of Tibet: Wuhan, China University Geoscience Press, p. 240–244 (in Chinese with English abstract).
Yao, X.F., Tang, J.X., Li, Z.J., Deng, S.L., Ding, S., Hu, Z.H., and Zhang, Z., 2013, The redefinition of the ore-forming porphyry's age in Gaerqiong skarn-type gold-copper deposit, Western Bangong Lake–Nujiang River metallogenic belt, Xizang (Tibet): Geological Review, v. 59, p. 193–201.
Yin, J.X., Sun, X.X., and Wen, C.F., 1988, Xigaze Group-the Flysch in Xigaze Forearc Basin in the southern Tibet: Memoirs of the Institute of Geology, Institute of National Academics, v. 3, p. 96–118 (in Chinese with English abstract).
Zhang, H.F., Xu, W.C., Guo, J.Q., Zong, K.Q., Cai, H.M., and Yuan, H.L., 2007a, Indosinian orogenesis of the Gangdese terrane: Evidences from zircon U-Pb dating and petrogenesis of granitoids: Earth Science Journal China University Geoscience, v. 32, p. 155–166.
Zhang, H.F., Xu, W.C., Guo, J.Q., Zong, K.Q., Cai, H.M., and Yuan, H.L., 2007b, Zircon U-Pb and Hf isotopic composition of deformed granite in the southern margin of the Gangdese belt, Tibet: Evidence for Early Jurassic subduction of Neo-Tethyan oceanic slab: Acta Petrologica Sinica, v. 23, no. 6, p. 1347–1353 (in Chinese with English abstract).

Zhang, L.L., Liu, C.Z., Wu, F.Y., Ji, W.Q., and Wang, J.G., 2013, Zedong terrane revisited: An intra-oceanic arc within Neo-Tethys or a part of the Asian active continental margin?: Journal of Asian Earth Sciences, v. 80, p. 34–55, doi:10.1016/j.jseaes.2013.10.029.

Zhao, T.P., Zhou, M.F., Zhao, J.H., Zhang, K.J., and Chen, W., 2008, Geochronology and geochemistry of the c. 80 Ma Rutog granitic pluton, northwestern Tibet: Implications for the tectonic evolution of the Lhasa terrane: Geological Magazine, v. 145, p. 845–857, doi:10.1017/S0016756808005025.

Zhou, C.Y., Zhu, D.C., Zhao, Z.D., Xu, J.F., Wan, L.Q., Chen, H.H., Xie, L.W., Dong, G.C., and Zhou, S., 2008, Petrogenesis of Daxiong pluton in western Gangdese, Tibet: Zircon U-Pb dating and Hf isotopic constraints: Acta Geologica Sinica, v. 24, p. 348–358.

Zhu, D.C., Pan, G.T., Chung, S.L., Liao, Z.L., Wang, L.Q., and Li, G.M., 2008, SHRIMP zircon age and geochemical constraints on the origin of Lower Jurassic volcanic rocks from the Yeba Formation, southern Gangdese, south Tibet: International Geology Review, v. 50, no. 5, p. 442–471, doi:10.2747/0020-6814.50.5.442.

Zhu, D.C., Zhao, Z.D., Niu, Y.L., Dilek, Y., and Mo, X.X., 2011, Lhasa terrane in southern Tibet came from Australia: Geology, v. 39, no. 8, p. 727–730, doi:10.1130/G31895.1.

Zhu, D.C., Zhao, Z.D., Niu, Y.L., Dilek, Y., Hou, Z.Q., and Mo, X.X., 2013, The origin and pre-Cenozoic evolution of the Tibetan Plateau: Gondwana Research, v. 23, p. 1429–1454, doi:10.1016/j.gr.2012.02.002.

Ziabrev, S., Aitchison, J., Abrajevitch, A., Davis, A., and Luo, H., 2003, Precise radiolarian age constraints on the timing of ophiolite generation and sedimentation in the Dazhuqu terrane, Yarlung–Tsangpo suture zone, Tibet: Journal of the Geological Society of London, v. 160, no. 4, p. 591–599, doi:10.1144/0016-764902-107.

Ziabrev, S.V., Aitchison, J.C., Abrajevitch, A.V., Davis, A.M., and Luo, H., 2004, Bainang terrane, Yarlung–Tsangpo suture, southern Tibet (Xizang, China): A record of intra-Neotethyan subduction–accretion processes preserved on the roof of the world: Journal of the Geological Society of London, v. 161, no. 3, p. 523–539, doi:10.1144/0016-764903-099.

Science Editor: Christian Koeberl
Associate Editor: Peter A. Cawood

Manuscript Received 22 October 2013
Revised Manuscript Received 18 April 2014
Manuscript Accepted 16 May 2014

Printed in the USA